

8-31-1990

Comparative analysis of single and double dwell acquisition schemes

Gurinder Singh Ahluwalia
New Jersey Institute of Technology

Follow this and additional works at: <https://digitalcommons.njit.edu/theses>



Part of the [Electrical and Electronics Commons](#)

Recommended Citation

Ahluwalia, Gurinder Singh, "Comparative analysis of single and double dwell acquisition schemes" (1990). *Theses*. 2434.

<https://digitalcommons.njit.edu/theses/2434>

This Thesis is brought to you for free and open access by the Electronic Theses and Dissertations at Digital Commons @ NJIT. It has been accepted for inclusion in Theses by an authorized administrator of Digital Commons @ NJIT. For more information, please contact digitalcommons@njit.edu.

Copyright Warning & Restrictions

The copyright law of the United States (Title 17, United States Code) governs the making of photocopies or other reproductions of copyrighted material.

Under certain conditions specified in the law, libraries and archives are authorized to furnish a photocopy or other reproduction. One of these specified conditions is that the photocopy or reproduction is not to be “used for any purpose other than private study, scholarship, or research.” If a user makes a request for, or later uses, a photocopy or reproduction for purposes in excess of “fair use” that user may be liable for copyright infringement,

This institution reserves the right to refuse to accept a copying order if, in its judgment, fulfillment of the order would involve violation of copyright law.

Please Note: The author retains the copyright while the New Jersey Institute of Technology reserves the right to distribute this thesis or dissertation

Printing note: If you do not wish to print this page, then select “Pages from: first page # to: last page #” on the print dialog screen

The Van Houten library has removed some of the personal information and all signatures from the approval page and biographical sketches of theses and dissertations in order to protect the identity of NJIT graduates and faculty.

ABSTRACT

Title of Thesis: Comparative Analysis of Single and Double Dwell Acquisition Systems
Gurinder Singh Ahluwalia, Master of Science in Electrical Engineering, 1990
Thesis directed by: Professor Joseph Frank

Single and double dwell pseudonoise (PN) acquisition systems are described, explained and analyzed. These systems are designed to synchronize a locally generated PN signal with a received PN signal of unknown phase in the presence of noise. The mean, variance and an approximate probability distribution function (PDF) of the acquisition time for the single and double dwell PN acquisition schemes is developed. Intuitively, the double dwell acquisition system should be superior to the single dwell system because of the ability to quickly dismiss incorrect cells and further verify probable hits. It is shown analytically that this is in fact true and that a double dwell system greatly reduces (36%) the expected acquisition time over a single dwell system.

The generating functions for both acquisition schemes are found via signal-flow diagrams. In order to compare the two systems, it is necessary to evaluate the effect of the penalty, K (false alarm penalty), which is done via state-transition diagrams. The mean and variance for both schemes are found in terms of: probability of detection, probability of false alarm, false alarm penalty and dwell times. Finally, a general expression for the PDF is found for both acquisition systems.

It is shown that the double dwell acquisition scheme can significantly reduce the expected acquisition time from that obtained with a single dwell system.

2) Comparative Analysis of Single and Double Dwell Acquisition Schemes

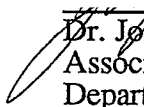
1) By
Gurinder Singh Ahluwalia

Thesis submitted to the Faculty of the Graduate School
of the New Jersey Institute of Technology in partial fulfillment
of the requirements for the degree of
Master of Science in Electrical Engineering
1990

Title of Thesis: Comparative Analysis of Single and Double Dwell Acquisition Schemes

Name of Candidate: Gurinder Singh Ahluwalia
Master of Science in Electrical Engineering, 1990

Thesis and Abstract Approved:

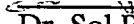


Dr. Joseph Frank
Associate Professor
Department of Electrical Engineering

7/23/90
Date

Dr. Stanley Reisman
Professor
Department of Electrical Engineering

7/23/90
Date



Dr. Sol Rosenstark
Professor
Department of Electrical Engineering

7/25/90
Date

VITA

Name: Gurinder Singh Ahluwalia

Permanent Address:

Degree and Date to be Conferred: Master of Science in Electrical Engineering, 1990

Date of birth:

Place of birth:

Secondary Education: Pearl River High School, 1983

<u>Collegiate Institutions attended</u>	<u>Dates</u>	<u>Degree</u>	<u>Date of Degree</u>
New York University	1983-87	B.S.	June 1987
The Cooper Union for the Advancement of Science and Art	1984-87	B.E.	May 1987
New Jersey Institute of Technology	1987-90	M.S.E.E.	October 1990

Major: Electrical Engineering

Positions held:

Production Planning Specialist, GE Magnetic Resonance Business Center - 1990
3200 N. Grandview Boulevard, Waukesha, Wisconsin 53188

Production Supervisor, ATF Flat Panel Displays, GE Aerospace - 1989
50 Fordham Road, Wilmington, Massachusetts

*To my parents
Daljit Singh and Deyinder Kaur Ahluwalia
for their never ending support*

Acknowledgements

I would like to thank Professor Joseph Frank for his valuable guidance and inspiration. I also thank Professors Stanley Reisman and Sol Rosenstark for their helpful suggestions.

I further would like to thank GE Medical Systems for their positive outlook on higher education and specifically in support of my graduate work.

Preface

The main objective of this work is to provide a quantitative comparison between two PN acquisition schemes. The two schemes that are analyzed are the single and double dwell acquisition systems.

The material on the single dwell system is a compilation and simplification of works that have been published by DiCarlo and Weber, and Holmes and Chen[1,7]. The background material as well as the section on lock-detector analysis can be found in both journals and textbooks. However, here it is written in a tutorial manner so that it can be easily understood and it provides the background for understanding the analysis of the double dwell system. In order to make the desired comparison, it was necessary to analyze the double dwell scheme using signal flow techniques and the reduction of the generating function. In the double dwell analysis, a close approximation of the pdf of the acquisition time is derived as well as the mean and variance of the time to acquisition. The pdf of the acquisition time for the double dwell system is a new result that has not been previously published.

In the concluding chapter, the results that were derived are presented. In order to make a useful quantitative comparison, two specific examples are analyzed numerically. In both cases, the results are shown graphically and it becomes apparent that the double dwell is superior to the single dwell. Finally, some insight is given pertaining to the results.

Table of Contents

I	Binary Phase Shift Keying Spread Spectrum System	1
1.1	Data and PN Code Modulation/Demodulation	2
1.2	Synchronization	5
1.2.1	Acquisition	6
1.2.2	Tracking	7
1.3	Carrier Recovery	9
1.3.1	Phase-Locked Loop	9
1.3.2	Squaring Loop	11
II	Mathematical Foundation of Direct Sequence Spread Spectrum Systems	13
2.1	Introduction	13
2.2	Characteristics of a Random Binary Sequence	13
2.3	PN Sequences	17
2.3.1	Maximal-length Sequences	17
2.3.2	Spreading Code: Autocorrelation Function	18
2.3.3	Spreading Code: Power Spectral Density	21
2.4	Product of a PN Code with a Delayed Replica	23
2.4.1	Spectral Analysis	24
2.5	Signal-Flow and State-Transition Diagrams	30
2.6	Application of the Z-Transform	34
2.7	Absorbing Markov Chains	38
2.7.1	Mean Time to Absorption	41
III	Direct Sequence PN Code Acquisition Schemes	44
3.1	Introduction	44
3.1.1	Single-Dwell Model Description	46
3.1.2	Analysis of Single-Dwell Acquisition	47
3.2	Lock-Detector Analysis	54
3.2.1	Evaluation of the Penalty: K	56
3.3	Double-Dwell Acquisition Scheme	57
3.3.1	Model Description	57
3.3.2	System Analysis	59
3.3.3	Acquisition Parameters	62
IV	Conclusions	71
4.1	System Comparisons	71
4.2	Recommendation for Future Work	76
	Appendices	77
	Appendix A	77
	Appendix B-1	79
	Appendix B-2	81
	Appendix B-3	82
	Selected Bibliography	83

Chapter 1

Binary Phase Shift Keying Spread Spectrum System

A spread spectrum communication system transmits information over a bandwidth which is much larger than that of the message signal. It is this spreading effect that gives rise to the name spread spectrum.

The motivation for reliable spread spectrum communication systems is manifold but can perhaps be summarized as follows. The sender wishes to transmit in such a way as to provide unintended receivers with as low probability of intercept (LPI) as is possible. Also, it is usually desirable that the receiver achieve a certain level of immunity from various forms of jamming. Finally, the system may be required to operate in a multiple-access environment. This can be achieved by using spreading codes with low cross-correlations so that an unintended receiver will detect the transmission only as noise and the intended receiver will be able to recover the signal by a “despreading” process.

In order to achieve the characteristics mentioned above, one must be willing to “pay the price.” In this case, a much larger transmission bandwidth than would ordinarily be required to transmit the message and a great deal of complexity in the transmitter/receiver. A less obvious tradeoff is the time required to achieve code synchronization so that the data may be demodulated.

A typical binary phase shift keying (BPSK) spread spectrum system is shown in Figure 1.1. This chapter will discuss various aspects of the transmitter/receiver system in order to prepare the reader for the detailed analysis that follows. First, data and spreading code modulation/demodulation is analyzed. Second, the concept of synchronization is introduced and discussed by separating the topics

of acquisition and tracking. The former will be investigated in detail in Chapter 3. Finally, in this chapter, a carrier recovery technique is reviewed for the sake of completeness.

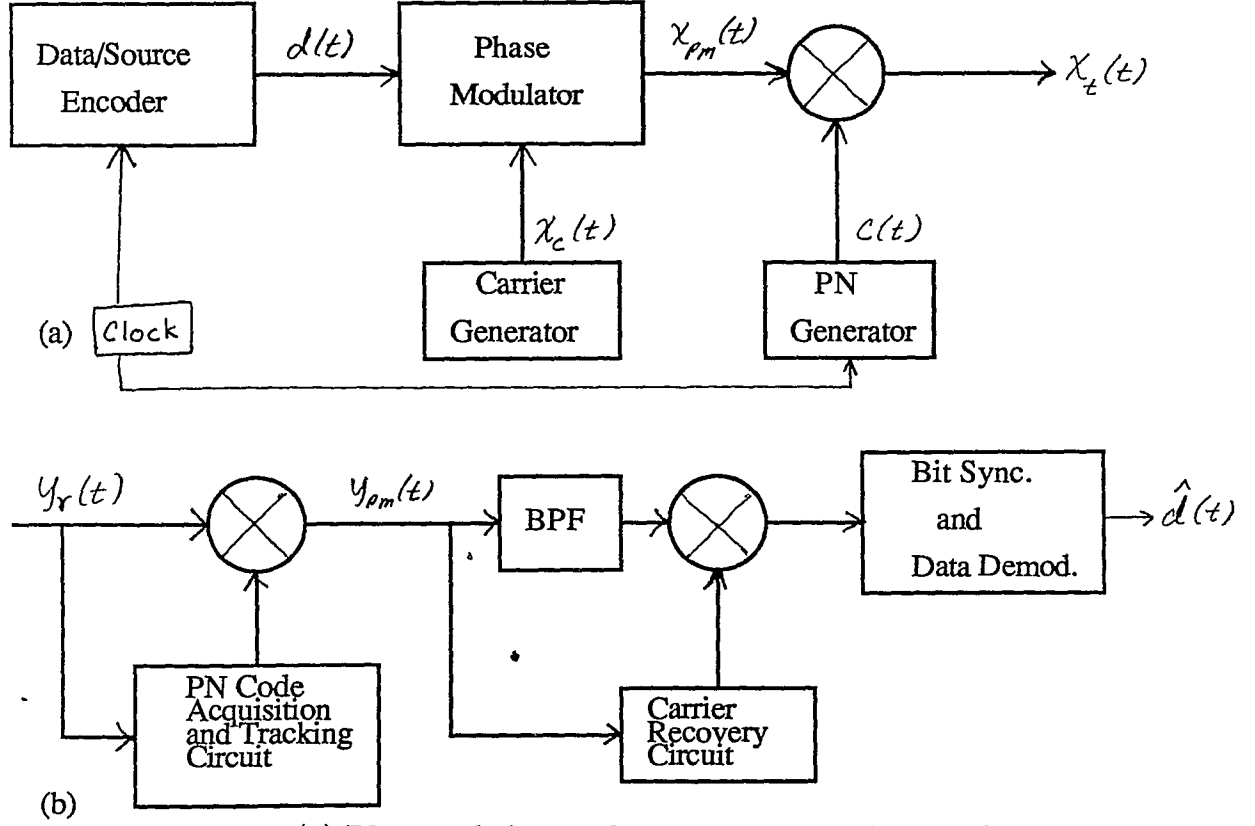


Figure 1.1 (a) PN encoded spread spectrum transmitter and
(b) coherent receiver

1.1 Data and PN Code Modulation/ Demodulation

The BPSK data and pseudonoise (PN) code modulator is shown in Figure 1.2. Consider the phase-modulated signal $x_{pm}(t)$ which is an ordinary BPSK signal which can be represented as

$$x_{pm}(t) = \sqrt{2P} \sin(\omega_o t + d_k \pi/2) \quad (1.1)$$

or equivalently,

$$x_{pm}(t) = \sqrt{2P}d_k \sin \omega_o t \quad (1.2)$$

$$nT_b \leq t < (n+1)T_b, \quad n = \text{integer}$$

where P = power of carrier signal

ω_o = carrier frequency

T_b = data bit duration

$d_k = 1$ or -1 corresponding to '1' or '0' respectively

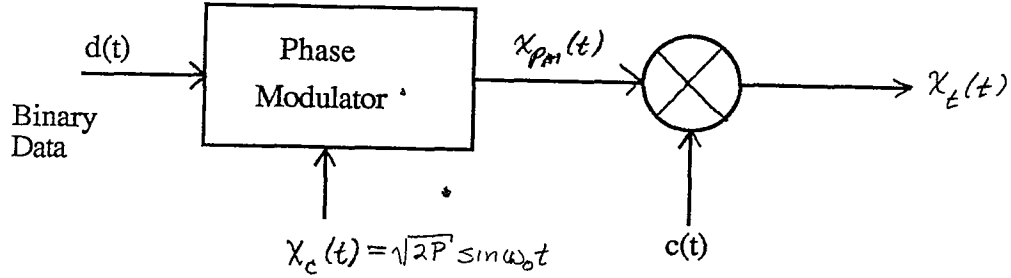


Figure 1.2 BPSK DS spread spectrum transmitter

It will be assumed throughout that the “message” bits (d_k) are statistically independent and take on the values ± 1 with equal probability.

The BPSK modulated signal is then “spread” by the PN sequence as illustrated in Figure 1.2. Analytically,

$$x_t(t) = x_{pm}(t)c(t) \quad (1.3)$$

where $c(t) = \pm 1$. The method of generation of the PN sequence is discussed in detail in Chapter 2. It is common for the rate of the PN sequence (chip rate) to be several orders of magnitude greater than that of the data. The chip duration,

T_c , is defined as:

$$T_c = \frac{T_b}{N} \quad (1.4)$$

where N is defined as the processing gain and its effect on the spectrum of the signal is discussed in section 2.3.2.

Rewriting Eq. (1.3),

$$\begin{aligned} x_t(t) &= c_\ell x_{pm}(t) \\ &= c_\ell \sqrt{2P} \sin(\omega_0 t + d_k \pi/2) \\ \ell T_c &< t < (\ell + 1)T_c, \quad \ell = \text{integer} \end{aligned} \quad (1.5)$$

Equivalently,

$$\begin{aligned} x_t(t) &= \sqrt{2P} \sin(\omega_0 t + d_k c_{kN+l} \pi/2) \\ &= d_k c_{kN+l} \sqrt{2P} \sin \omega_0 t \end{aligned} \quad (1.6)$$

where $kT_b + \ell T_c \leq t < (k+1)T_b + (\ell+1)T_c$

$$k = 0, 1, 2, \dots, N-1$$

$$N = \text{integer}$$

For the purpose of discussion, define

$$\begin{aligned} d(t) &= d_k & kT_b \leq t < (k+1)T_b \\ c(t) &= c_\ell & \ell T_c \leq t < (\ell+1)T_c \quad \text{for all integers } k, \ell \end{aligned} \quad (1.7)$$

Therefore, rewriting equation (1.6),

$$x_t(t) = d(t) c(t) \sqrt{2P} \sin \omega_0 t \quad (1.8)$$

Assuming the local PN sequence is synchronized with the received sequence and neglecting the effects of noise and phase ambiguity in the carrier, the receiver

shown in Figure 1.3 will be able to demodulate the carrier. Analytically,

$$\begin{aligned} y_{pm}(t) &= y_r(t) c(t) \\ &= d(t) c^2(t) \sqrt{2P} \sin \omega_0 t \end{aligned} \quad (1.9)$$

Note that

$$c^2(t) = 1 \quad \text{for all } t \quad (1.10)$$

thereby Eq. (1.9) can be simplified to

$$y_{pm}(t) = d(t) \sqrt{2P} \sin \omega_0 t \quad (1.11)$$

and $d(t)$ can be easily recovered by a standard BPSK demodulator.

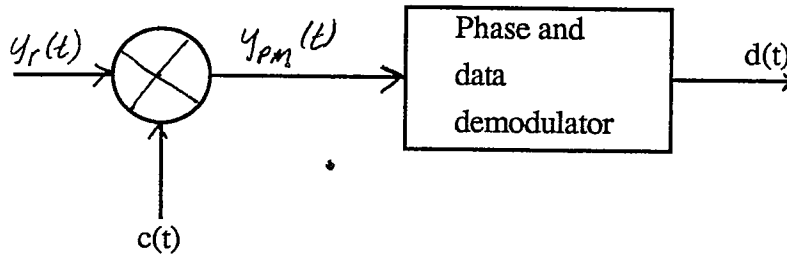


Figure 1.3 Coherent BPSK receiver

1.2 Synchronization

In the previous section, it was assumed that the received and locally generated PN sequences were synchronized and the effect of noise was neglected. Normally, synchronization must be achieved at the receiver by first acquiring the phase of the PN sequence and once acquired, it must be tracked to within at least $(1/2)T_c$. This whole operation must be done in the presence of noise, in the following analysis additive white Gaussian noise (AWGN) is assumed. In this section, the problem of acquisition will be briefly discussed; two possible acquisition schemes and their performance is analyzed in detail in chapter 3. This section is concluded with an analysis of a noncoherent code tracking circuit.

1.2.1 Acquisition

Various strategies to acquire the phase of the spreading code can be implemented. However, in low signal-to-noise applications, serial search techniques outperform the others[1] and it is this technique that is analyzed, specifically, single dwell and multiple dwell schemes are investigated in chapter 3.

In order to analytically describe the performance of the single and multiple dwell schemes, it is necessary to understand signal flow graph techniques (section 2.3). It is also desirable to evaluate the penalty for false-lock which can be facilitated through the use of Absorbing Markov Chains (section 2.4). In the remainder of this section, the intent is to give the reader motivation for what follows in Chapter 3.

Assuming no a priori information about the received PN code phase, the probability that the current search will yield the correct cell is $1/q$ where q is the number of cells (the number of chips in one period of the PN sequence). It is assumed that the search is advanced in increments of T_c , the chip duration. With some thought, it can be shown that if a hit does not occur in the first $k - 1$ cells then

$$\begin{aligned} P(k^{th} \text{ cell hit} \mid \text{no hit in } k - 1 \text{ cells}) &= \frac{1}{q - (k - 1)} \\ &= \frac{1}{q - k + 1} \end{aligned} \quad (1.12)$$

Due to noise considerations, it is possible (with probability P_{FA}) that the acquisition system may detect a hit when in fact a miss should have been detected. In order to model the acquisition system properly, if the receiver does incorrectly detect a hit, a penalty should be imposed to represent the time lost due to false-lock. The representation and analysis of this penalty is studied in Section 3.2.1. Even more detrimental to the performance of the system is if the

system fails to detect a hit. For if this happens, the entire sequential search has to be repeated since none of the remaining cells can yield a true hit. When the code phase is acquired to within $(1/2)T_c$, the tracking circuit is activated.

1.2.2 Tracking

Once the signal is acquired to within one-half of a code chip, it is the function of the code tracking loop to insure that the locally generated PN sequence remains synchronized with the received PN sequence.

Assuming the received signal is in the presence of AWGN, $n(t)$, it can be represented as

$$y_r(t) = \sqrt{2P}d(t-T)c(t-T)\sin(\omega_0 t + \theta) + n(t) \quad (1.13)$$

where T represents the transmission delay and θ is the random carrier phase. From Figure 1.4, the received signal is despread in two different channels. In this particular case, the channels have a code phase difference of one code chip, T_c . It is shown in Appendix A-1 that the error signal can be approximated by

$$e_\epsilon \approx \frac{2P\epsilon}{T_c} \quad (1.14)$$

where $\epsilon = T - \hat{T}$.

From Eq. (1.14) and Figure 1.4, the operation of the tracking circuit is explained (qualitatively) in the remainder of this section.

For the sake of discussion, assume that $\hat{T} < T$ which implies that $\epsilon > 0$. This means that the estimated delay, \hat{T} , is too short and must be increased. From Figure 1.4 it can be seen that the late channel contains some compensation for local PN sequence while the early channel causes the sequence phase difference to be even greater. Due to the greater correlation in the late channel, the output of the summer will be positive. This will cause the voltage-controlled clock

to increase the delay thereby providing continuous tracking of the received PN sequence. Notice in Figure (1.14) the multiplier and bandpass filter act as a correlator. If $c(t - T)$ and $c(t - \hat{T})$ are closely correlated then the output of the

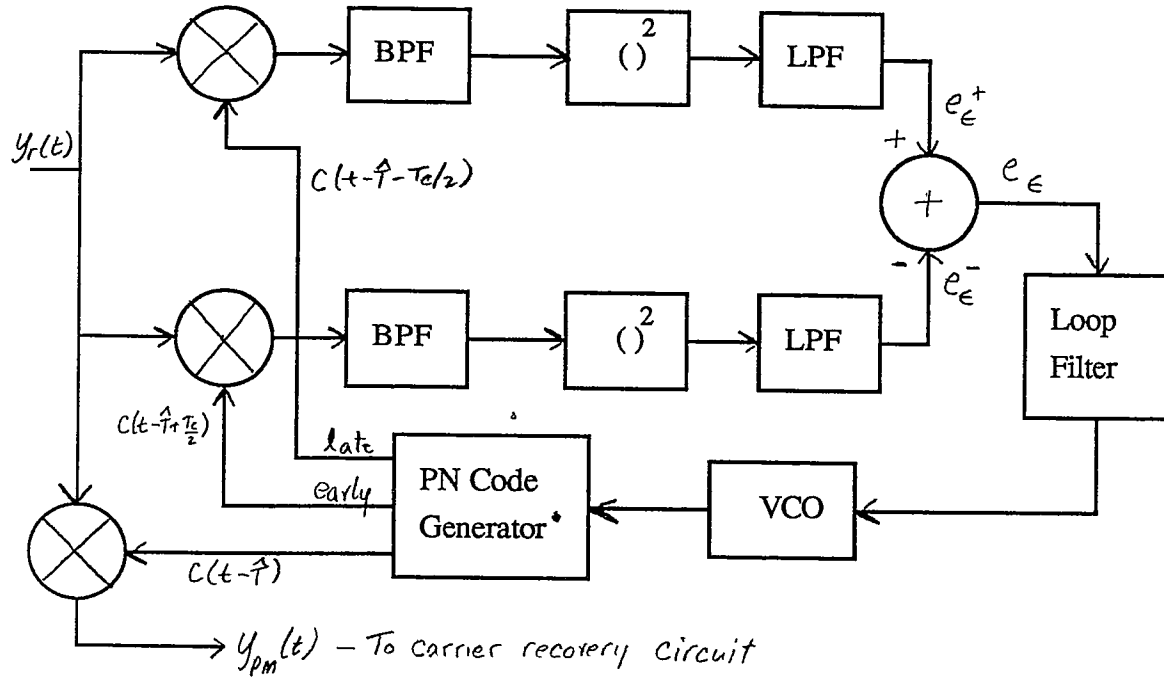


Figure 1.4 Full-time early-late noncoherent code tracking loop

multiplier will collapse into the data modulated carrier at f_0 . Since $\frac{1}{T_d} \ll \frac{1}{T_c}$, the signal will be despread enough so that the change in the dc output of the lowpass filter (cutoff frequency, f_H should be much lower than f_0) will be detectable. The above described process will enable the signal going to the carrier recovery circuit to be

$$\begin{aligned} y_{pm}(t) &= y_r(t) c(t - \hat{T}) \\ &= \sqrt{2P} d(t - T) \sin(\omega_0 t + \theta) \quad \text{assuming } \hat{T} = T \end{aligned} \quad (1.15)$$

Having the received code and locally generated code synchronized, the signal

must be carrier demodulated. In order to do this, it is necessary to recover the carrier and this is discussed in the next section.

1.3 Carrier Recovery

As in the case of synchronization of PN sequences, it is imperative for the receiver to recover the carrier phase. This recovery of phase can be accomplished by means of a squaring loop[2] such as that shown in Figure 1.5. Since the squaring loop employs a phase-locked loop (PLL), the latter will be discussed in the next section in order to obtain a better understanding of the recovery circuit.

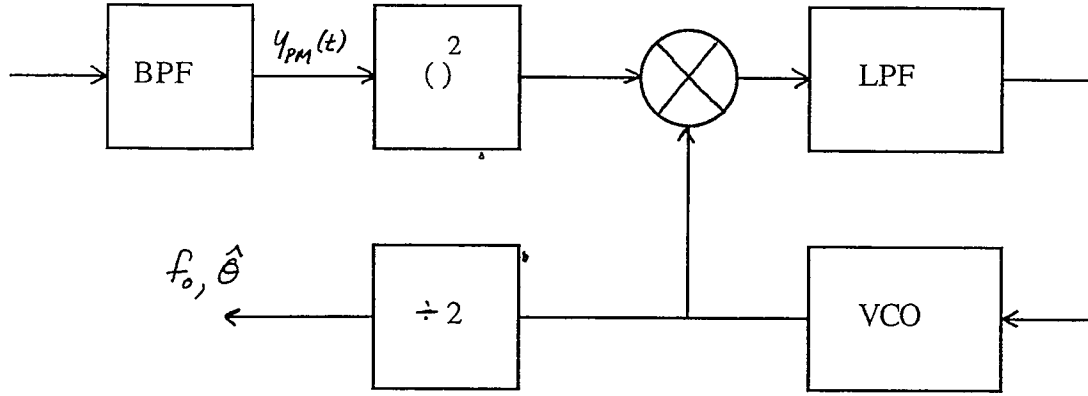


Figure 1.5 Squaring-Loop for carrier recovery.

1.3.1 Phase-Locked Loop

The device shown in Figure 1.6, a phase-locked loop, allows for the recovery of the phase of the received carrier. In the following analysis, the received signal is assumed noiseless with a carrier frequency f_0 and phase θ . The received signal is multiplied by the output of the voltage-controlled oscillator (VCO). The VCO output (estimated carrier frequency) varies linearly with the applied input voltage, $e(t)$. The operation of the VCO can be characterized by the following

$$\frac{d}{dt}\hat{\theta}(t) = k_1 e(t) + k_2 \quad (1.16)$$

In order to analyze the PLL for phase recovery, the phase error is defined as

$$\phi(t) = \theta(t) - \hat{\theta}(t) \quad (1.17)$$

differentiating with respect to time yields,

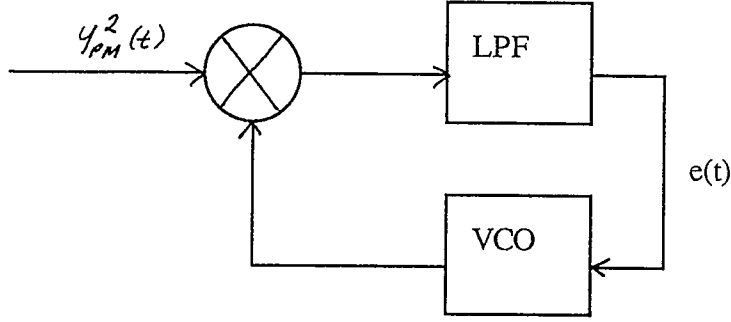


Figure 1.6 Block diagram of a phase-locked loop.

$$\dot{\phi}(t) = \dot{\theta}(t) - \frac{d}{dt}\hat{\theta}(t) \quad (1.18)$$

From the linearized model of the PLL shown in Figure 1.7 and Eq. (1.16), the above equation can be rewritten as follows

$$\dot{\phi}(t) = \dot{\theta}(t) - C \int_0^t h(t - \tau) \phi(\tau) d\tau \quad (1.19)$$

The linearization is justifiable when the phase error is small enough so that $\sin \phi \approx \phi$. Taking the Laplace transform of Eq. (1.19) yields,

$$s\phi(s) = s\theta(s) - CH(s)\phi(s) \quad (1.20)$$

where $H(s)$ is the transfer function of the loop filter. Substituting the transform of Eq. (1.17) into Eq. (1.20) allows the transfer function of the phase to be found. With algebraic manipulation,

$$\frac{\hat{\theta}(s)}{\theta(s)} = \frac{CH(s)}{s + CH(s)} \quad (1.21)$$

Essentially, the phase-locked loop acts as a narrowband filter, tracking the frequency of the received signal. It requires that a spectral line be present at that frequency. Thus, a qualitative description in the next section of a squaring-loop will show how this can be accomplished.

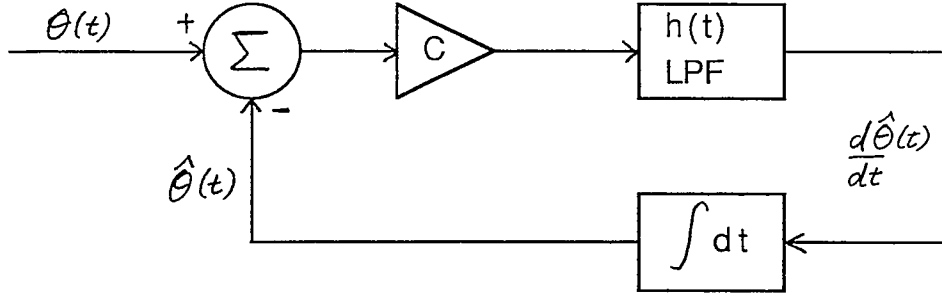


Figure 1.7 Linearized model of phase-locked loop shown in Figure 1.6

1.3.2 Squaring Loop ,

Recall Eq. (1.15) which describes an ideally synchronized PN sequence. This synchronized signal is ready to be data demodulated with an appropriate carrier. Notice in Figure 1.5 that the despread signal is band-pass filtered. This is done because once the PN sequence is synchronized, the signal recomposes itself to an ordinary BPSK bandpass signal. The filter should therefore have a center frequency of f_0 and a bandwidth of $2B_d$ where B_d is the bandwidth of the baseband data signal $d(t)$. This carrier must be recovered and a qualitative explanation is given here.

Rewriting Eq. (1.15),

$$y_{pm}(t) = \sqrt{2P}d(t - T)\sin(\omega_0 t + \theta) \quad (1.22)$$

it can be seen that if the frequency, f_0 and phase, θ can be tracked then it will be possible to accurately demodulate the signal. Since the data modulation scheme

is BPSK, passing the signal through a squaring circuit shown in Figure 1.5 yields

$$y_{pm}^2(t) = P[1 + \cos(2\omega_0 t + 2\theta)] \quad (1.23)$$

Eq. 1.23 contains a spectral line at $2f_0$ and can be tracked using the PLL described in the previous section. From this PLL, f_0 and $\hat{\theta}$ can be estimated. It should be pointed out that the divide by two circuit of Figure 1.5 causes a phase ambiguity ($\pm\pi$) in the output. This phase ambiguity problem is present in all phase modulation schemes and can be overcome by special encoding (such as differential encoding).

Chapter 2

Mathematical Foundation of Direct Sequence Spread Spectrum Systems

This chapter introduces and fully explains the various mathematical concepts and analytical tools necessary for the evaluation of different code acquisition techniques. Most of the techniques that are needed are explained here and used as a basis for the analysis that is carried out in the next chapter.

2.1 Introduction

When designing a spread spectrum system, it would be most desirable from the point of view of security to have a spreading code that consisted of a purely random binary sequence. However, this would require that both the transmitter and receiver have an infinite storage for the sequence. Due to this impossibility, a pseudorandom (PN) sequence is selected that has certain properties. These properties will be examined in section 2.3 after discussing the characteristics of a purely random binary sequence in section 2.2.

The remainder of this chapter deals with signal-flow graphs and absorbing Markov chains. They are explained in detail and used to aid in the analysis and determination of the performance of the acquisition systems presented in chapter 3.

2.2 Characteristics of a Random Binary Sequence

Before discussing PN sequences, it is useful to first investigate and determine certain characteristics of a random binary wave as shown in Figure 2.1. The symbols 1 and 0 are represented by $+A$ and $-A$ volts respectively.

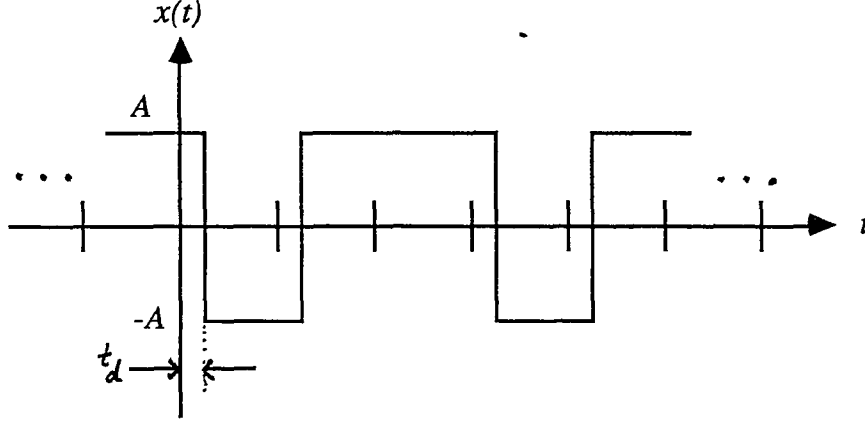


Figure 2.1 Random binary sequence with random starting phase.

Since the binary wave (sequence) is random, and

$$P(x(t) = -A) = P(x(t) = A) = \frac{1}{2} \quad (2.1)$$

it follows that $E[x(t)] = 0$ and $\overline{x(t)} \neq 0$ where $E[\]$ represents ensemble averaging and the overbar indicates time averaging. The autocorrelation is found from

$$R_x(t_1, t_2) = E[x(t_1)x(t_2)] \quad (2.2)$$

and can be divided into two regions. If $|t_1 - t_2| > T$ where T is the duration of one bit, then the two samples are independent and Eq. (2.2) becomes

$$\begin{aligned} R_x(t_1, t_2) &= E[x(t_1)] E[x(t_2)] \\ &= 0 \end{aligned} \quad (2.3)$$

If however $|t_1 - t_2| \leq T$ the analysis is not as simple since the samples are not necessarily independent. One can note that when $t_1 - t_2 = 0$, $R_x(0) = A^2$ is the maximum. If the condition that $|t_1 - t_2| < T - t_d$ and $t_1 = 0$ is imposed, then it follows that

$$E[x(t_1)x(t_2)] = \begin{cases} A^2 & \text{if } |t_1 - t_2| < T - t_d \\ 0 & \text{otherwise} \end{cases} \quad (2.4)$$

Averaging this result over possible values of t_d yields

$$\begin{aligned} R_x(t_1, t_2) &= E[x(t_1)x(t_2)] \\ &= \int_0^{t'_d} A^2 f_{t_d} dt_d \end{aligned} \quad (2.5)$$

where f_{t_d} is the probability density function of the starting phase and is defined as

$$f_{t_d}(t) = \begin{cases} \frac{1}{T} & 0 < t < T \\ 0 & \text{otherwise} \end{cases} \quad (2.6)$$

Using Eq. (2.6) and the fact that $t'_d = T - |t_1 - t_2|$ in Eq. (2.5) results in,

$$\begin{aligned} R_x(t_1, t_2) &= \int_0^{T-|t_1-t_2|} A^2 \frac{1}{T} dt_d \\ &= \frac{A^2}{T} (T - |t_1 - t_2|) \\ &= A^2 \left(1 - \frac{|t_1 - t_2|}{T}\right) \quad \text{for } |t_1 - t_2| < T \end{aligned} \quad (2.7)$$

Since the autocorrelation depends only on the difference of t_1 and t_2 , Eq. (2.7) can be rewritten as

$$R_x(\tau) = \begin{cases} A^2 \left(1 - \frac{|\tau|}{T}\right) & |\tau| < T \\ 0 & \text{otherwise} \end{cases} \quad (2.8)$$

where $\tau = |t_1 - t_2|$. This relation, plotted in Figure 2.2, could also have been derived using the Weiner-Khintchine relation. In fact, this relation will be used to derive and sketch the power spectral density (PSD) of the random binary wave.

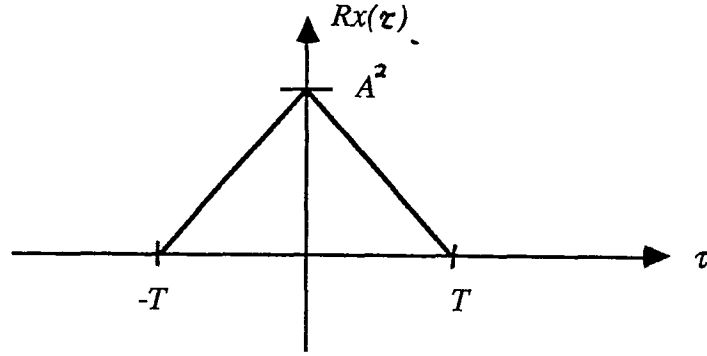


Figure 2.2 Autocorrelation of the random binary sequence shown in Fig. 2.1

The Fourier transform pair

$$S_x(f) = \int_{-\infty}^{\infty} R_x(\tau) \exp(-j2\pi f\tau) d\tau \quad (2.9)$$

•

$$R_x(\tau) = \int_{-\infty}^{\infty} S_x(f) \exp(j2\pi f\tau) df \quad (2.10)$$

are considered the Wiener-Khintchine relations. From Eq. (2.9) it can be seen that if the autocorrelation function is transformable then the transform (with respect to τ) is the PSD of that function. In this case, from Eq. (2.8) and (2.9), the transform is directly found to be

$$S_x(f) = A^2 T \text{sinc}^2(fT) \quad (2.11)$$

where A is the amplitude and T is the duration of the random binary pulse (see Figure 2.3).

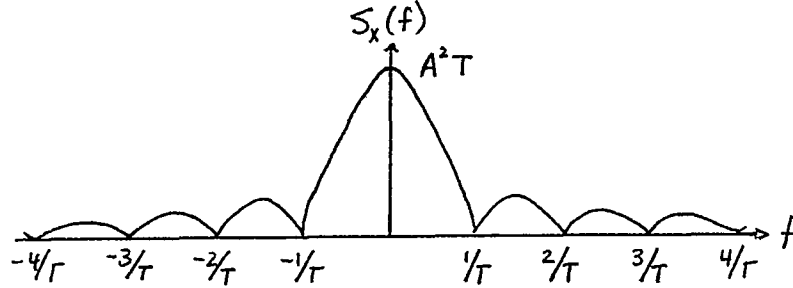


Figure 2.3 PSD of the random binary sequence of Fig. 2.1

2.3 PN Sequences

As explained in the introduction, since it is not possible to use a purely random binary sequence as a spreading code, some suboptimal sequence must be used. This sequence will have some noiselike properties but will also possess other properties which are discussed in this section.

2.3.1 Maximal-length Sequences

A linear maximal sequence is a shift register sequence having the largest possible period for a specific register length. The period is given by

$$N = 2^m - 1 \quad (2.12)$$

where m is the number of stages. For example, in Figure 2.4, $m = 3$ and $N = 7$. Assuming the initial state of the sequence to be $R_0 = 1$, $R_1 = 0$, $R_2 = 0$ yields the following output sequence:

$$0011101 \quad 00111010011101$$

where the first period is shown slightly separated from the rest for the sake of clarity. The adder shown in Figure 2.4 is a modulo-2 (exclusive or) adder and

also notice that the initial state of the registers can be anything but the all zero sequence. Using this simple example, the following properties of m-sequences can be seen (see Appendix B-1):

- I A maximal sequence has one more 1 than 0.
- II The sum (modulo-2) of two phase-shifted versions of an m-sequence yields the same sequence but shifted.
- III The discrete autocorrelation of an m-sequence is two-valued.

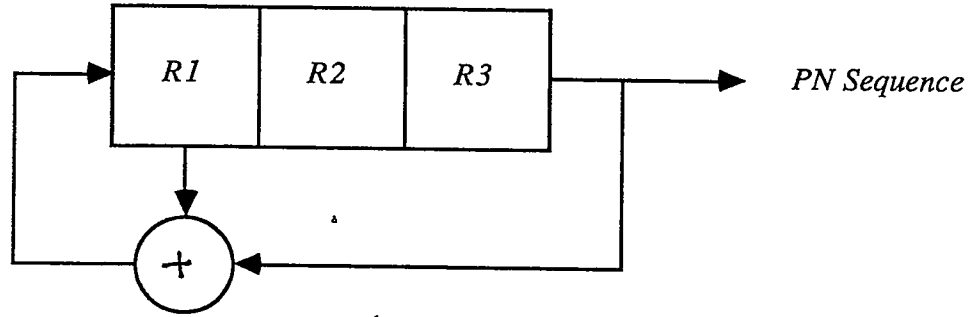


Figure 2.4 Three-stage maximal-length sequence generator

2.3.2 Spreading Code: Autocorrelation Function

Having shown some of the properties of maximal length sequences, the autocorrelation function and power spectral density of the sequences will be calculated. This knowledge together with the other sections of this chapter will facilitate the analysis of the acquisition schemes.

Recall, the autocorrelation function for a deterministic signal is given by

$$R_c(\tau) = \frac{1}{T} \int_0^T c(t) c(t + \tau) dt \quad (2.13)$$

where $c(t)$ is defined by Eq. (1.7) and is rewritten as

$$c(t) = \sum_{\ell=-\infty}^{\infty} c_{\ell} p(t - \ell T_c) \quad (2.14)$$

where $p(t)$ is a unit pulse whose amplitude is unity and duration is from $t = 0$ until $t = T_c$ and c_ℓ is either ± 1 . Substituting Eq. (2.14) into (2.13) yields

$$R_c(\tau) = \frac{1}{T} \int_0^T \sum_{i=-\infty}^{\infty} c_i p(t - iT_c) \sum_{j=-\infty}^{\infty} c_j p(t - jT_c + \tau) dt \quad (2.15)$$

This can be rewritten as

$$R_c(\tau) = \frac{1}{T} \sum_{i=-\infty}^{\infty} c_i \sum_{j=-\infty}^{\infty} c_j \int_0^T p(t - iT_c) p(t - jT_c + \tau) dt \quad (2.16)$$

In Eq. (2.16), τ can take on any value. Define

$$\tau' = \tau - nT_c \quad (2.17)$$

where n is an integer such that $|\tau'| < T_c$. Rewriting Eq. (2.16) with τ' yields

$$R_c(\tau') = \frac{1}{T} \sum_{i=-\infty}^{\infty} c_i \sum_{j=-\infty}^{\infty} c_{j+n} \int_0^T p(t - iT_c) p(t - (j+n)T_c + \tau') dt \quad (2.18)$$

where τ' is a function of τ and n . In Eq. (2.18) it can be seen that the integrand is nonzero only when the pulses overlap. Analytically, only when $j = i + n$ and when $j = i + n + 1$ do the pulses overlap. Using Eq. (2.18) with this and the fact that $T = NT_c$, the double summation reduces into the following two single summation terms.

$$\begin{aligned} R_c(\tau') &= \frac{1}{NT_c} \sum_{i=-\infty}^{\infty} c_i c_{i+n} \int_{iT_c}^{(i+1)T_c - \tau'} p(t - iT_c) p(t - iT_c + \tau') dt \\ &\quad + \frac{1}{NT_c} \sum_{i=-\infty}^{\infty} c_i c_{i+n+1} \int_{(i+1)T_c - \tau'}^{(i+1)T_c} p(t - iT_c) p(t - (i+1)T_c + \tau') dt \end{aligned} \quad (2.19)$$

Substituting $\eta = t - iT_c$ into the integrals simplifies the result to

$$\begin{aligned} R_c(\tau') &= \frac{1}{T_c} \sum_{i=-\infty}^{\infty} c_i c_{i+n} \int_0^{T_c - \tau'} p(\eta) p(\eta + \tau') d\eta \\ &\quad + \frac{1}{T_c} \sum_{i=-\infty}^{\infty} c_i c_{i+n+1} \int_{T_c - \tau'}^{T_c} p(\eta) p(\eta - T_c + \tau') d\eta \end{aligned} \quad (2.20)$$

From Appendix (B-1), using Eq. (B-2) for PN sequences,

$$\begin{aligned}
R_c(\tau') &= r_c(n) \frac{1}{T_c} \int_0^{T_c - \tau'} p(\eta) p(\eta + \tau') d\eta \\
&\quad + r_c(n+1) \frac{1}{T_c} \int_{T_c - \tau'}^{T_c} p(\eta) p(\eta - T_c + \tau') d\eta
\end{aligned} \tag{2.21}$$

where $r_c(n)$ is the discrete two-valued autocorrelation function of $c(t)$. Since $p(t)$ is a known pulse, the integral yields

$$R_c(\tau') = r_c(n) \left[\frac{1}{T_c} (T_c - \tau') \right] \tag{2.22}$$

where τ' and n are defined in Eq. (2.17). Using Eq. (B-3) and Eq. (2.22), it is possible to divide the autocorrelation function into two regions. When $0 \leq |\tau| \leq T_c$ then Eq. (2.22) reduces to

$$\begin{aligned}
R_c(\tau) &= r_c(0) \left[1 - \frac{|\tau|}{T_c} \right] + r_c(1) \frac{|\tau|}{T_c} \\
&= 1 - \frac{N+1}{NT_c} |\tau|
\end{aligned} \tag{2.23}$$

and when $T_c \leq |\tau'| \leq (N-1)T_c$ then

$$R_c(\tau) = r_c(k) \left(1 - \frac{|\tau'|}{T_c} \right) + r_c(k+1) \frac{|\tau'|}{T_c} \tag{2.24}$$

where k and $k+1$ are not integer multiples of N and $\tau' = \tau - kT_c$ which insures $|\tau'| > T_c$. Substituting the values of the discrete autocorrelation function into Eq. (2.24) yields

$$\begin{aligned}
R_c(\tau) &= -\frac{1}{N} \left(1 - \frac{|\tau'|}{T_c} + \frac{|\tau'|}{T_c} \right) \\
&= -\frac{1}{N}
\end{aligned} \tag{2.25}$$

These results, Eq. (2.23) and (2.25) are plotted for $c(t)$ in Figure 2.5.

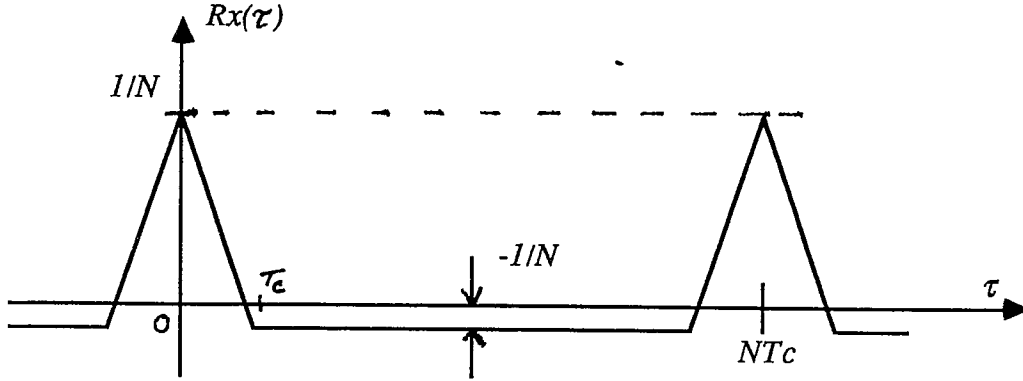


Figure 2.5 Autocorrelation function of a maximal-length sequence.

2.3.3 Spreading Code: Power Spectral Density

In order to find the power spectral density (PSD) of the spreading code $c(t)$, the Wiener-Khinchine relation can be used as follows

$$S_c(f) = \int_{-\infty}^{\infty} R_c(\tau) \exp(-j2\pi f\tau) d\tau \quad (2.26)$$

But $R_c(\tau)$ is periodic therefore the following transform pair will aid in the analysis

$$g_p(t) = \sum_{n=-\infty}^{\infty} g(t - nT_o) \leftrightarrow \frac{1}{T_o} G(f) \sum_{n=-\infty}^{\infty} \delta(f - \frac{n}{T_o}) \quad (2.27)$$

where $g(t) = g_p(t) = R_c(t)$ for $-T_o/2 \leq t \leq T_o/2$ in this case and $T_o = NT_c$. Note that in the above equation, $G(f)$ is the Fourier transform of $g(t)$. Therefore, it is necessary to evaluate the transform of $g(t)$. In this case, the Fourier transform (with respect to τ) of $R_c(\tau)$ $-T_o/2 \leq \tau \leq T_o/2$ is needed. From the basic transform relationship

$$G(f) = \int_{-\infty}^{\infty} g(t) \exp(-j2\pi ft) dt \quad (2.28)$$

it is possible to find S_{c_1} (the PSD of one period of the autocorrelation function) as follows.

$$S_{c_1} = \int_{-T_o/2}^{T_o/2} R_{c_1}(\tau) \exp(-j2\pi f\tau) d\tau \quad (2.29)$$

Notice that in Eq. (2.29) the limits have been reduced from Eq. (2.26). This is because $R_{c_1}(\tau)$ is one period of the autocorrelation function centered at the origin. Substituting Eq. (2.23) and (2.25) into Eq. (2.29) yields

$$S_{c_1}(f) = \int_{-T_o/2}^{-T_c} \frac{1}{N} \exp(-j2\pi f\tau) d\tau + \int_{-T_c}^0 \left(1 + \frac{N+1}{T_o} \tau\right) \exp(-j2\pi f\tau) d\tau \\ + \int_0^{T_c} \left(1 - \frac{N+1}{T_o} \tau\right) \exp(-j2\pi f\tau) d\tau + \int_{T_c}^{T_o/2} -\frac{1}{N} \exp(-j2\pi f\tau) d\tau \quad (2.30)$$

This can be simplified (see Appendix (B-2)) yielding,

$$S_{c_1}(f) = -T_o \operatorname{sinc}(fT_o) + \frac{(N+1)T_c}{N} \operatorname{sinc}^2(fT_c) \quad (2.31)$$

Recall that Eq. (2.31) is the PSD of a non-periodic function and only when Eq. (2.27) is used does the result apply to the periodic (autocorrelation) function. Substitution yields,

$$S_c(f) = \frac{1}{T_o} S_{c_1}(f) \sum_{n=-\infty}^{\infty} \delta\left(f - \frac{n}{T_o}\right) \quad (2.32)$$

which can be reduced (see Appendix B-3) to

$$S_c(f) = -\frac{1}{N} \delta(f) + \frac{(N+1)}{N_2} \sum_{n=-\infty}^{\infty} \operatorname{sinc}^2(fT_c) \delta\left(f - \frac{n}{NT_c}\right) \quad (2.33)$$

Upon inspection of Eq. (2.33) it can be seen that the spectrum is discrete which follows from the fact that the function is periodic and the dc term is $+\frac{1}{N^2}$. The latter can be obtained from Eq. (2.33) by setting $n = 0$. Eq. (2.33) is plotted in Figure 2.6

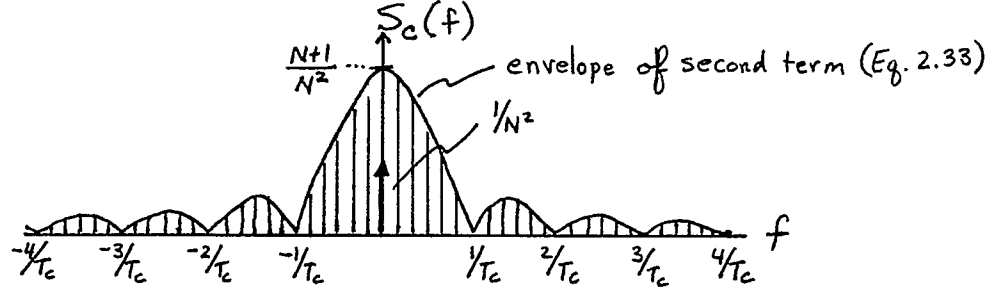


Figure 2.6 Power spectral density of $c(t)$.

2.4 Product of a PN Code with a Delayed Replica

In order to detect when the received and locally generated spreading codes are synchronized, the receiver must be able to detect a change in the spectral content of the “despread signal.” This idea will become clearer as the spectrum characteristics are developed and explained in the following section.

There are four distinct cases which can arise during the synchronization process. First, if the received and locally generated codes are exactly synchronized ($\epsilon = 0$). Second, if the delay (difference in code phase) is less than one code chip ($|\epsilon| < T_c$). Third, if the delay is exactly a multiple of a code chip ($|\epsilon| = kT_c$ where $k = 1, 2, \dots, N - 1$) and finally, if the phase difference is greater than one chip but less than a period so that $T_c < |\epsilon| < (N - 1)T_c$ where NT_c is the period of the spreading code. These different phase delays are analyzed below by keeping the analysis as independent of the value of ϵ as is possible and then the results are discussed for different ϵ and are illustrated in Figure 2.12.

2.4.1 Spectral Analysis

If the received and locally generated spreading codes are represented by $c(t)$ and $c(t + \epsilon)$ respectively, then the autocorrelation of the product is

$$R_{cc'}(\tau, \epsilon) = \frac{1}{T_o} \int_0^{T_o} c(t)c(t + \epsilon)c(t + \tau)c(t + \epsilon + \tau)dt \quad (2.34)$$

This calculation is difficult if done directly. In figure 2.7, by

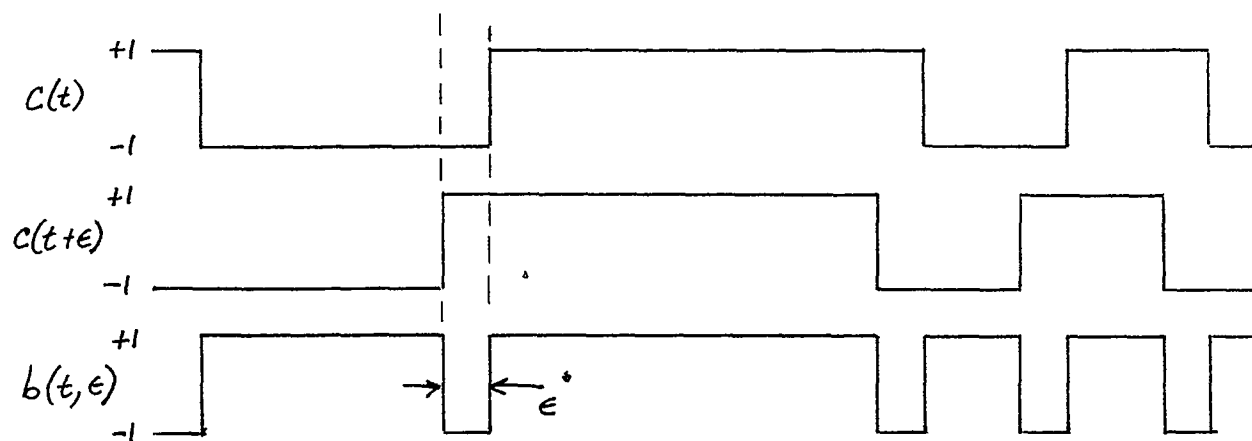


Figure 2.7 Product of maximal-length sequences (see Ref. 3)

following [8], where

$$b(t, \epsilon) = c(t)c(t + \epsilon) \quad (2.35a)$$

the autocorrelation is written as

$$R_b(\tau, \epsilon) = \frac{1}{T_o} \int_0^{T_o} b(t, \epsilon)b(t + \tau, \epsilon)dt \quad (2.35b)$$

where $b(t, \epsilon)$ can be written as the sum of $p(t, \epsilon)$ and $q(t, \epsilon)$ and both are periodic with period T_c and NT_c respectively. These functions are shown in Figure 2.8 and the autocorrelation calculation follows.

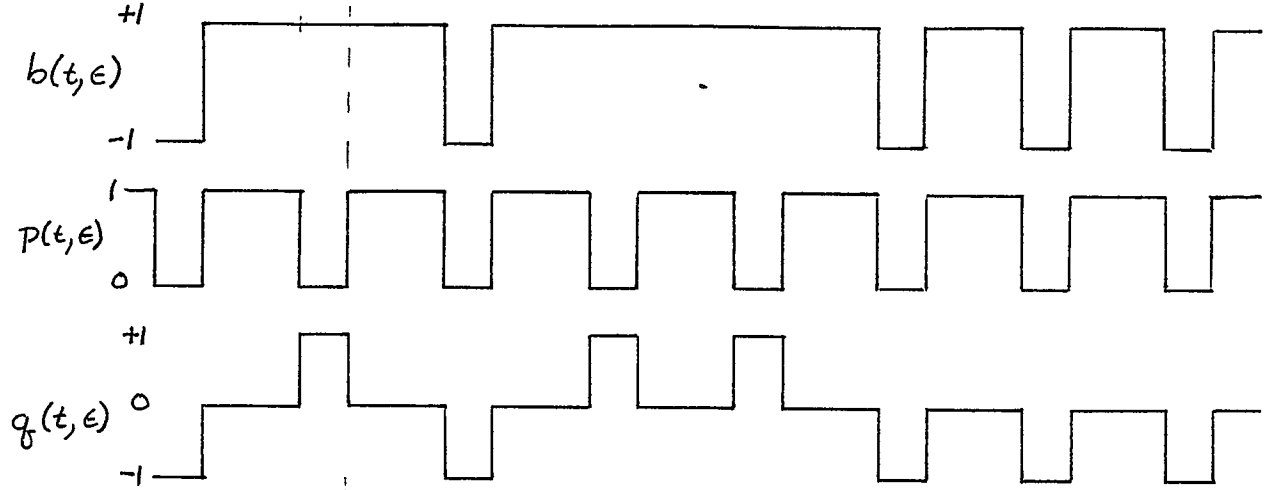


Figure 2.8 Decomposition of the product of m-sequences (see Ref. 3)

Rewriting Eq. (2.35b) using the following,

$$b(t, \epsilon) = p(t, \epsilon) + q(t, \epsilon) \quad (2.36)$$

yields

$$R_b(\tau, \epsilon) = R_p(\tau, \epsilon) + R_q(\tau, \epsilon) + R_{pq}(\tau, \epsilon) + R_{qp}(\tau, \epsilon) \quad (2.37)$$

where $p(t, \epsilon)$ is just a binary pulse with period T_c and duration of $T_c - \epsilon$ and $q(t, \epsilon)$ is a three-valued function, with period NT_c , such that Eq. (2.36) will hold. This relation is shown in Figure 2.8. The right-hand side terms of Eq. (2.37) can be found by using a combination of graphical as well as analytical means. Evaluating $R_p(\tau, \epsilon)$, the autocorrelation of a periodic pulse with duration $T_c - \epsilon$, from Figure 2.8 yields,

$$R_p(\tau, \epsilon) = R_0(\epsilon) + \frac{|\epsilon|}{T_c} \sum_{n=-\infty}^{\infty} \Lambda(\tau - nT_c, |\epsilon|) \quad (2.38a)$$

for $|\epsilon| < T_c/2$ where $R_0(\epsilon) = 1 - 2(|\epsilon|/T_c)$ and $\Lambda(\tau, |\epsilon|)$ is defined as

$$\Lambda(\tau, |\epsilon|) \equiv 1 - |\tau/\epsilon|$$

and for $T_c/2 \leq |\epsilon| \leq T_c$,

$$R_p(\tau, \epsilon) = \left(1 - \frac{|\epsilon|}{T_c}\right) \sum_{n=-\infty}^{\infty} \Lambda(\tau - nT_c, T_c - |\epsilon|) \quad (2.38b)$$

These autocorrelations are plotted in Figure 2.9. Notice for $|\epsilon| < T_c/2$, there is a constant term of $1 - 2(|\epsilon|/T_c)$ which is represented by $R_0(\epsilon)$ in Eq. (2.38a).

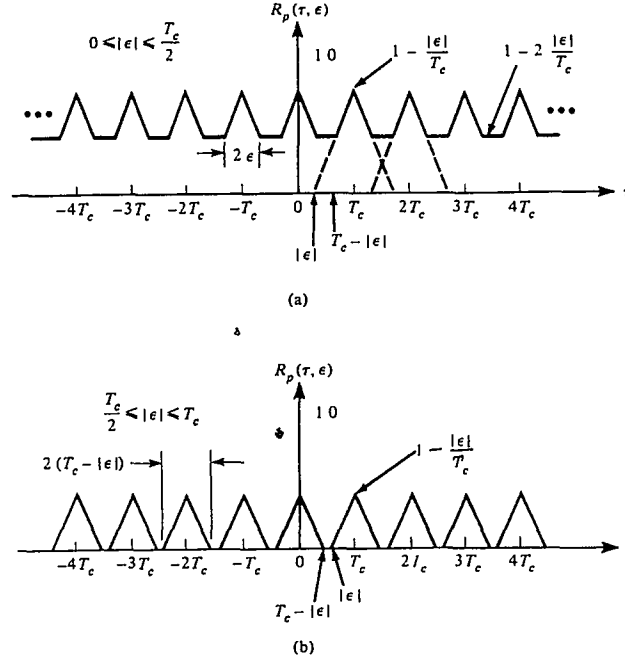


Figure 2.9 Autocorrelation of $p(t, \epsilon)$ (a) $|\epsilon| \leq T_c$
(b) $T_c/2 \leq |\epsilon| < T_c$ (see Ref. 8)

Similarly, the autocorrelation $R_q(\tau, \epsilon)$ is found by inspection of Figure 2.8 and is plotted in Figure 2.10. Notice that $q(\tau, \epsilon)$ is just a phase-shifted version of the spreading code with a shorter duration. This reduced duration causes the autocorrelation to be slightly different from the function plotted in Figure 2.5. As with $R_p(\tau, \epsilon)$ the autocorrelation function can be explicitly written for the two regions as:

$$\begin{aligned}
R_q(\tau, \epsilon) &= \left(1 + \frac{1}{N}\right) \frac{|\epsilon|}{T_c} \sum_m \Lambda(\tau - mNT_c, |\epsilon|) \\
&\quad - \frac{|\epsilon|}{NT_c} \sum_n \Lambda(\tau - nT_c, |\epsilon|)
\end{aligned} \tag{2.39a}$$

for $|\epsilon| < T_c/2$ and

$$\begin{aligned}
R_q(\tau, \epsilon) &= \left(1 + \frac{1}{N}\right) \frac{|\epsilon|}{T_c} \sum_m \Lambda(\tau - mNT_c, |\epsilon|) \\
&\quad - \frac{1}{N} \left(2 \frac{|\epsilon|}{T_c} - 1\right) - \frac{1}{N} \left(1 - \frac{|\epsilon|}{T_c}\right) \sum_n \Lambda(\tau - nT_c, T_c - |\epsilon|)
\end{aligned} \tag{2.39b}$$

for $T_c/2 \leq |\epsilon| \leq T_c$. Having found the autocorrelation of $p(t, \epsilon)$ and $q(t, \epsilon)$ only the cross-correlation remains to have a complete “picture” of the autocorrelation function of the product of the PN sequences ($R_b(\tau, \epsilon)$).

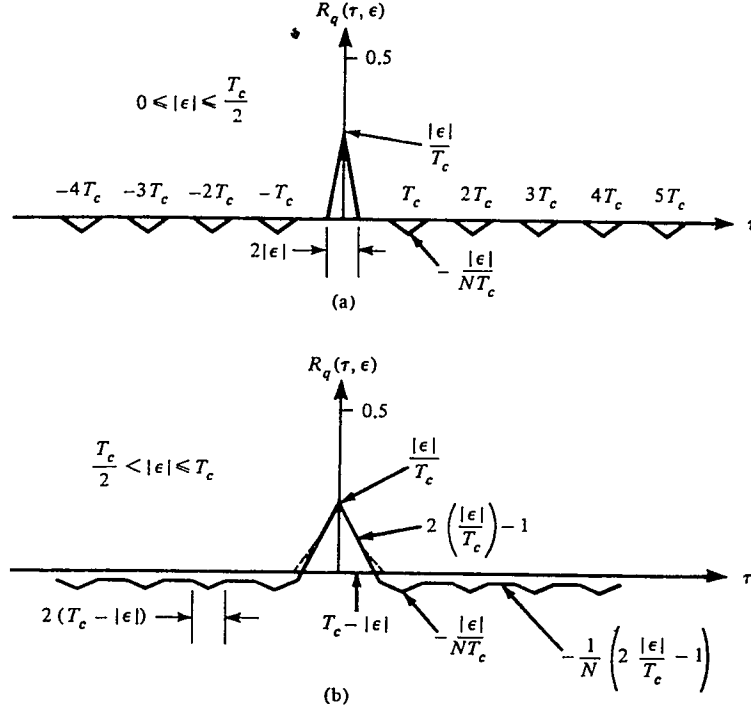


Figure 2.10 Autocorrelation of $q(t, \epsilon)$ (a) $|\epsilon| \leq T_c/2$

(b) $T_c/2 \leq |\epsilon| < T_c$ (see Ref. 8)

From the definition of the cross-correlation function,

$$R_{pq}(\tau, \epsilon) = \frac{1}{NT_c} \int_0^{NT_c} p(t, \epsilon) q(t + \tau, \epsilon) dt \quad (2.40)$$

If the substitution of $\lambda = t + \tau$ is made,

$$R_{pq}(\tau, \epsilon) = \frac{1}{NT_c} \int_{\tau}^{\tau+NT_c} p(\lambda - \tau, \epsilon) q(\lambda, \epsilon) d\lambda \quad (2.41)$$

then it is seen that the right-hand side is just the cross-correlation $R_{qp}(-\tau, \epsilon)$ so that

$$R_{pq}(\tau, \epsilon) = R_{qp}(-\tau, \epsilon) \quad (2.42)$$

As with the autocorrelation, the cross-correlation $R_{pq}(\tau, \epsilon)$ can be found directly from Figure 2.8 and is shown in Figure 2.11.

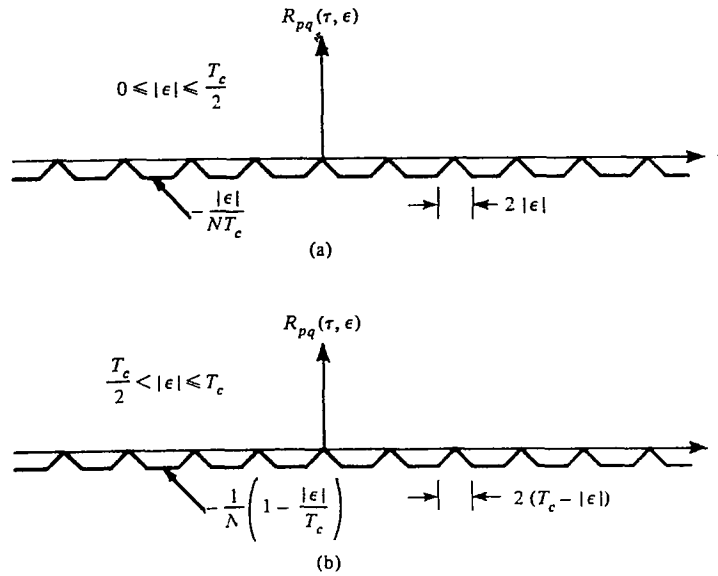


Figure 2.11 Cross-correlation: (a) $|\epsilon| \leq T_c$

(b) $T_c/2 \leq |\epsilon| < T_c$ (see Ref. 8)

Having found the four terms of Eq. (2.37), it is possible, with the aid of the Wiener-Khintchine relation, to find the power spectrum of the product of the

spreading codes ($c(t)$ and $c(t + \epsilon)$). Using Eq. (2.27) with the results obtained above, the transform of $R_b(\tau, \epsilon)$ is obtained and when simplified yields,

$$\begin{aligned}
S_b(f) = & [1 - (1 + \frac{1}{N})(\frac{|\epsilon|}{T_c})]^2 \delta(f) \\
& + (1 + \frac{1}{N})(\frac{|\epsilon|}{T_c^2}) \sum_{n=-\infty}^{\infty} \text{sinc}^2(n f_c |\epsilon|) \delta(f - n f_c) \\
& + (\frac{N+1}{N^2})(\frac{|\epsilon|}{T_c})^2 \sum_{m=-\infty}^{\infty} \text{sinc}^2(\frac{m f_c}{N} |\epsilon|) \delta(f - \frac{m f_c}{N}) \quad (2.43)
\end{aligned}$$

In Figure 2.12, Eq. (2.43) is plotted for different values of $|\epsilon| < T_c$. Notice when $\epsilon = 0$, the sequence are in perfect synchronization and the power spectrum is just a single line at $f = 0$. This is intuitively correct since $c^2(t) = 1$ is just a dc signal. Also in the figure, the spectrum is discrete and the spacing is dependent on ϵ . In fact, the synchronization process will exploit this characteristic.

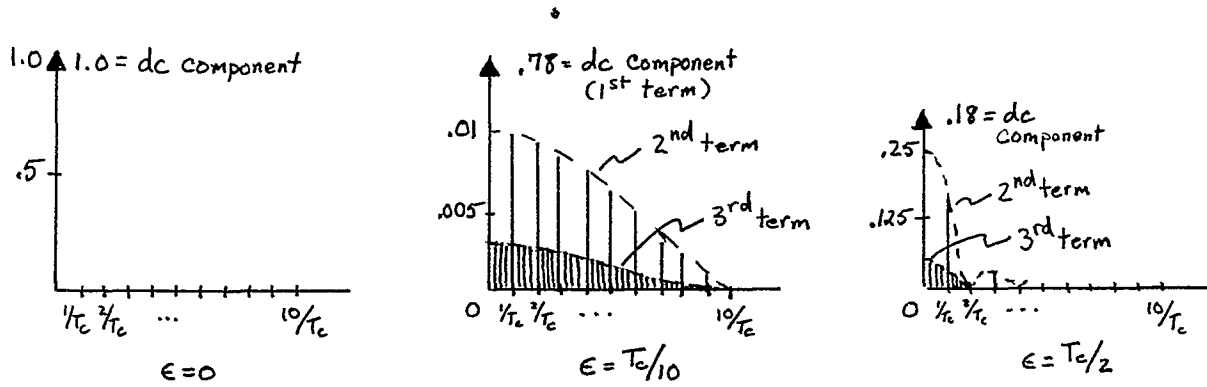


Figure 2.12 PSD of $b(t, \epsilon)$ for various $|\epsilon| \leq T_c/2$

If $\epsilon = kT_c$ then the product $b(t, \epsilon)$ will have the same spectrum as $c(t)$. This can be obtained from section 2.3.1 which states that the modulo-2 sum or equivalently, the product of two identical but phase-delayed maximal-length sequences is the same sequence but shifted [3].

Finally, for displacements of $kT_c < \epsilon < (k+1)T_c$, the power spectral density

becomes

$$S_b(f, \epsilon) = \frac{(\epsilon - kT_c)^2}{T_c} \text{sinc}^2 \pi f(\epsilon - kT_c) + \frac{((k+1)T_c - \epsilon)^2}{T_c} \text{sinc}^2 \pi f((k+1)T_c - \epsilon) \quad (2.44)$$

2.5 Signal-Flow and State-Transition Diagrams

In order to facilitate the evaluation of the acquisition system described in the next chapter, it is useful to understand the basic methods of signal-flow and state-transition diagrams.

A signal-flow diagram is a graphic representation of a set of linear equations. It allows for rapid simplification using standard reduction methods or Mason's theorems [4,5]. In this section, several terms that are used in signal-flow diagrams are defined. Then an abbreviated list of signal-flow simplifications is presented and discussed. Finally, Mason's theorem is presented and an example is given to illustrate the power of this theorem.

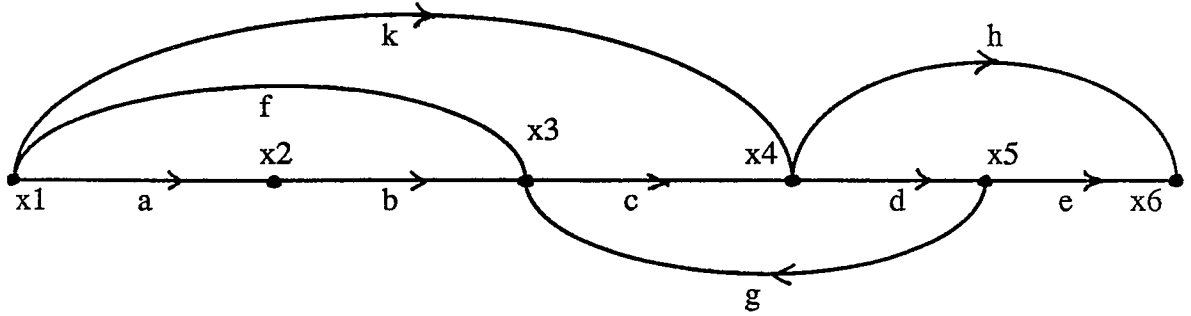


Figure 2.13 An example of a signal-flow diagram.

The following definitions refer to Figure 2.13 for illustration. A *source* (x_1) is a node having only outgoing branches. Similarly, a *sink* has only incoming branches (x_6). A *path* is a group of branches connected in one direction

(ab, fc, g). A path that originates from a source and terminates in a sink is the *path gain* ($abcde, kde, kdgch$), where the product of the coefficients is considered the gain ($x_1 \rightarrow x_2 : \text{path gain} = a$). A *feedback loop* originates and terminates at the same node ($x_3 \rightarrow x_4 \rightarrow x_5 \rightarrow x_3$). The product of the branches that form the feedback loop is considered the *loop gain* (cdg).

Having presented the fundamental terms used in signal-flow theory, it is appropriate to show (Figure 2.14) some of the basic reduction techniques[6].

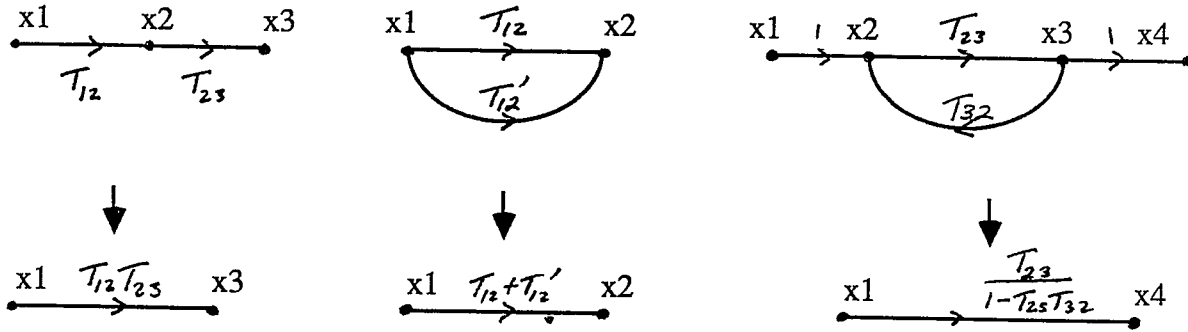


Figure 2.14 Reduction of the signal-flow diagram.

Although this technique is straightforward, for complicated or large systems it can become tedious. Mason's theorem, a more powerful technique is available which (almost by inspection) simplifies the signal-flow diagram into two nodes connected by a single branch. Using Mason's theorem[4,5], the general expression for signal-flow graph transfer function, H , is given by

$$H = \frac{\sum_j H_j \Delta_j}{\Delta} \quad (2.45)$$

where $\Delta = 1 - \sum T_1 + \sum T_2 - \dots + (-1)^m \sum T_m$.

T_1 = gain of each closed loop in the graph

- T_2 = product of the loop gain of any two nontouching closed loops
 T_m = product of the loop gain of any m nontouching closed loops
 H_j = gain of the j^{th} forward path
 Δ_j = value of Δ remaining when the path producing H_j is removed

A proof of this gain formula can be found in Reference 5. Here, an example is given to illustrate the application of Eq. (2.45).

From Figure (2.15),

$$\Delta = 1 - T_{33} - T_{34}T_{45}T_{53}$$

$$T_1 = T_{12}T_{23}T_{34}T_{45}T_{56}T_{67}$$

$$T_2 = T_{12}T_{24}T_{45}T_{56}T_{67}$$

$$T_3 = T_{12}T_{24}T_{46}T_{67}$$

$$T_4 = T_{12}T_{23}T_{34}T_{46}T_{67}$$

$$\Delta_1 = 1$$

$$\Delta_2 = 1 - T_{33}$$

$$\Delta_3 = 1 - T_{33}$$

$$\Delta_4 = 1$$

Substituting the above values into Eq. (2.45) we obtain

$$H = \frac{H_1\Delta_1 + H_2\Delta_2 + H_3\Delta_3 + H_4\Delta_4}{\Delta} \quad (2.46)$$

The technique just discussed is used widely in control theory but can also be applied to various problems as long as they are well defined. In this case, the technique will be used to allow for the simplification of the state-transition diagram shown in Fig. 2.16.

Substituting the above values into Eq. (2.45) we obtain

$$H = \frac{H_1\Delta_1 + H_2\Delta_2 + H_3\Delta_3 + H_4\Delta_4}{\Delta} \quad (2.46)$$

The technique just discussed is used widely in control theory but can also be applied to various problems as long as they are well defined. In this case, the technique will be used to allow for the simplification of the state-transition diagram.

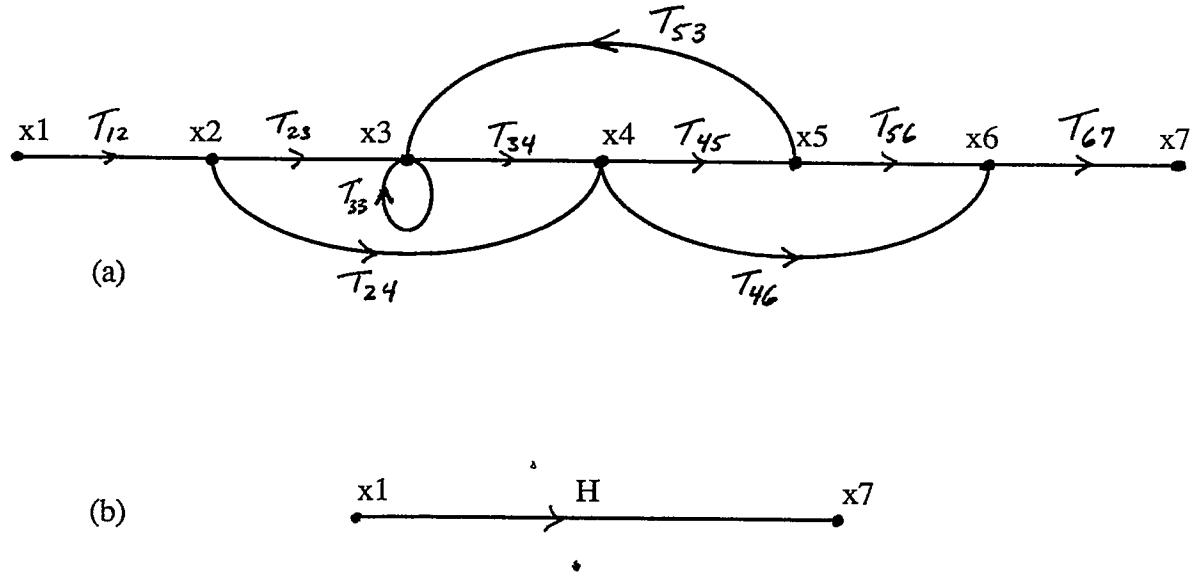


Figure 2.15 (a) Signal-flow example (b) reduced equivalent

Consider the following discrete three-state process:

$$P(x_3/x_1) = 0 \quad P(x_3/x_2) = 9/16 \quad P(x_3/x_3) = 1 \quad (2.47a)$$

$$P(x_2/x_1) = 1/4 \quad P(x_2/x_2) = 0 \quad P(x_2/x_3) = 0 \quad (2.47b)$$

$$P(x_1/x_1) = 3/4 \quad P(x_1/x_2) = 7/16 \quad P(x_1/x_3) = 0 \quad (2.47c)$$

This process is shown in Figure 2.16 as a state-transition diagram where the branches are labelled with the corresponding transition probabilities. From the above stated probabilities or Figure 2.16, the probability of the next state in terms of the previous state can be found as follows:

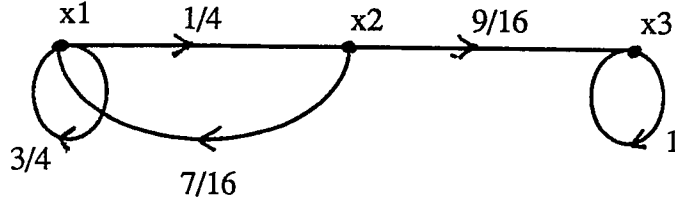


Figure 2.16 State transition diagram for the above described example

$$p_{x_1}(k+1) = P(x_1/x_1)p_{x_1}(k) + P(x_1/x_2)p_{x_2}(k) + P(x_1/x_3)p_{x_3}(k) \quad (2.48)$$

$$p_{x_2}(k+1) = P(x_2/x_1)p_{x_1}(k) + P(x_2/x_2)p_{x_2}(k) + P(x_2/x_3)p_{x_3}(k) \quad (2.49)$$

$$p_{x_3}(k+1) = P(x_3/x_1)p_{x_1}(k) + P(x_3/x_2)p_{x_2}(k) + P(x_3/x_3)p_{x_3}(k) \quad (2.50)$$

Since Eqs. (2.48-50) are linear, constant coefficient difference equations, it is possible and useful to take the Z-transform of them and work in the transform domain. However the results can only be useful if the transformed equation (state-transition diagram) and the original equations (state-transition diagrams) produce the same Markov chain. It is shown in [7] that this is in fact the case and it is therefore analytically proper to work in the transform domain.

2.6 Application of the Z-Transform

The Z-transform of the discrete probability function $p_{ij}(k)$ is

$$Z[p_{ij}(k)] = P_{ij}(z) = \sum_{k=0}^{\infty} z^k p_{ij}(k) \quad (2.51)$$

Notice that the series converges for $|z| < 1$. If Eq. (2.51) is differentiated with respect to z , and evaluated for $z = 1$,

$$\frac{\partial}{\partial z} P_{ij}(z)|_{z=1} = \sum_{k=0}^{\infty} k z^{k-1} p_{ij}(k)|_{z=1} = \sum_{k=0}^{\infty} k p_{ij}(k) \quad (2.52)$$

it can be noticed that this is just the mean number of steps to go from state i to j in the process. This can be rewritten as

$$\bar{T}_{ij} = \sum_{k=0}^{\infty} k p_{ij}(k) \quad (2.53)$$

where the overbar represents the mean and it is assumed that one step equals one unit of time. Similarly, the variance (σ_{ij}^2) of the time required to go from state i to state j is found as follows. Taking the random variable T_{ij} , the variance is just

$$\begin{aligned} \sigma_{ij}^2 &= E[T_{ij}^2] - E^2[T_{ij}] \\ &= E[T_{ij}^2] - \bar{T}_{ij}^2 \end{aligned} \quad (2.54)$$

However $E[T_{ij}^2]$ can be found by first differentiating Eq. (2.51) twice (w.r.t. z) and simplifying:

$$\begin{aligned} \frac{\partial^2}{\partial z^2} P_{ij}(z) &= \frac{\partial}{\partial z} \left[\sum_{k=0}^{\infty} k z^{k-1} p_{ij}(k) \right] \\ &= \sum_{k=0}^{\infty} k(k-1) p_{ij}(k) \\ &= \sum_{k=0}^{\infty} k^2 p_{ij}(k) - \sum_{k=0}^{\infty} p_{ij}(k) \end{aligned} \quad (2.55)$$

Rearranging this equation and realizing that it can be written as follows

$$E[T_{ij}^2] = \frac{\partial^2}{\partial z^2} P_{ij}(z)|_{z=1} + \frac{\partial}{\partial z} P_{ij}(z)|_{z=1} \quad (2.56)$$

and substituting this into Eq. (2.54) yields,

$$\sigma_{ij}^2 = \frac{\partial^2}{\partial z^2} P_{ij}(z)|_{z=1} - \left(\frac{\partial}{\partial z} P_{ij}(z)|_{z=1} \right)^2 + \frac{\partial}{\partial z} P_{ij}(z)|_{z=1} \quad (2.57)$$

Having found both the mean and variance of the time required to move from state i to state j , it would also be informative to know the probability of the

"system" going from one particular state to another at a specified time or during a specified period of time. From [6],

$$p_{ij}(k) = \frac{1}{k!} \frac{d^k}{dz^k} P_{ij}(z)|_{z=0} \quad (2.58)$$

This equation can also be used to find the probability that the system is in some specified state by taking into account the different state possibilities. These concepts are made clearer with the following example. If the Z-transform of Figure 2.16 is taken, the following flow-graph is generated:

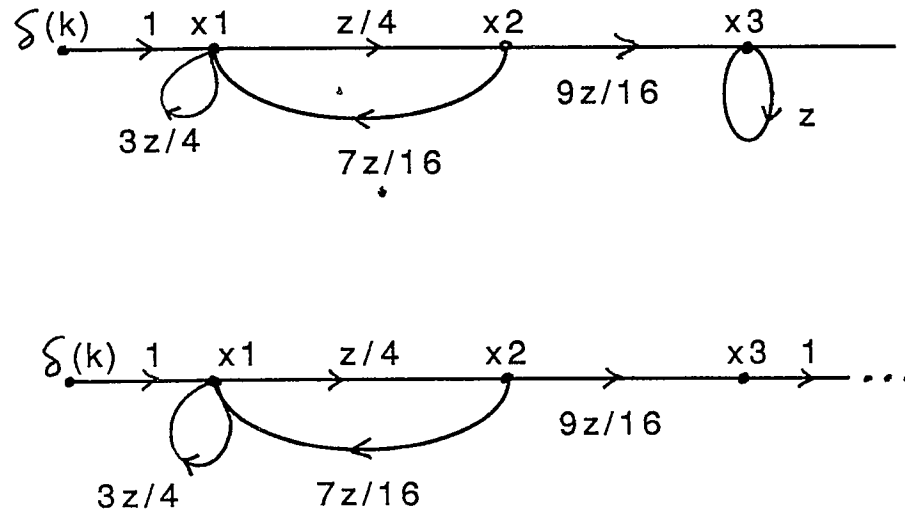


Figure 2.17 Example of a transformed flow-graph.

In Figure 2.17, x_3 is known as the absorbing state. Once this state is reached, the system will forever remain there. States x_1 , x_2 are transient states. Notice that x_1 is preceded by $\delta(n)$ and a unity branch. This takes the initial condition ($p_{x_1}(0) = 1$) into account. Using Mason's gain formula, explained in the previous section, the mean time for the system to go from state x_1 to x_3 can be found by

first finding the transfer function of Figure 2.17 (b).

$$P_{13}(z) = \frac{\sum_i \hat{T}_i \Delta_i}{\Delta}$$

where $T_1 = \frac{9}{64}z^2$, $\Delta_1 = 1$, $\Delta = 1 - \frac{3}{4}z - \frac{7}{64}z^2$

$$P_{13}(z) = \frac{\frac{9}{64}z^2}{1 - \frac{3}{4}z - \frac{7}{64}z^2} \quad (2.59)$$

substituting this into Eq. (2.52) and (2.53) yields

$$\begin{aligned} \bar{T}_{13} &= \frac{\partial}{\partial z} P_{13}(z)|_{z=1} \frac{(64 - 48z - 7z^2)(18z) + 9z^2(48 + 14z)}{(64 - 48z - 7z^2)^2} \Big|_{z=1} \\ &= \frac{80}{9} \end{aligned} \quad (2.60)$$

It is also useful to find the variance of the mean time the system will take to reach its absorbing state. Using Eq. (2.55),

$$\begin{aligned} \frac{\partial^2}{\partial z^2} P_{ij}(z) &= \frac{\partial}{\partial z} \left[\frac{(1 - \frac{3}{4}z - \frac{7}{64}z^2)(\frac{18}{64}z) + \frac{9}{64}z^2(\frac{3}{4} + \frac{14}{64}z)}{(1 - \frac{3}{4}z - \frac{7}{64}z^2)^2} \right] \\ &= \frac{(1 - \frac{3}{4}z - \frac{7}{64}z^2)(\frac{18}{64}(1 - \frac{3}{4}z)) + (\frac{3}{2} + \frac{28}{64}z)(\frac{18}{64}z - \frac{27}{256}z^2)}{(1 - \frac{3}{4}z - \frac{7}{64}z^2)^3} \end{aligned} \quad (2.61)$$

Evaluating this at $z = 1$ and substituting this results along with \bar{T}_{13} into Eq. (2.57) yields

$$\sigma_{13}^2 \approx 56$$

Another statistic which can be obtained from Figure 2.17a is the cumulative probability that the system has reached the absorbing state. This can also be found by using

$$P_{33}(k) = \sum_i \sum_{n=0}^{k-1} p_{i3}(n) \quad (2.62)$$

Notice that Eq. (2.62) would require that all transition probabilities be calculated. This tedious but correct computation can be avoided by, once again, using

Mason's gain formula (Eq. 2.45) on Figure 2.17a:

$$T_1 = \frac{1}{4}z \cdot \frac{9}{16}z = \frac{9}{64}z^2$$

$$\Delta_1 = 1$$

$$\Delta = 1 - \frac{3}{4}z - \frac{7}{64}z^2 - z + \frac{3}{4}z^2 + \frac{7}{64}z^3$$

yielding,

$$P_{33}(z) = \frac{\frac{9}{64}z^2}{(1-z)(1-\frac{7}{8}z)(1+\frac{1}{8}z)} \quad (2.63)$$

$$= \frac{1}{1-z} + \frac{-9/8}{1-\frac{7}{8}z} + \frac{1/8}{1-(\frac{-1}{8}z)}$$

where a partial fraction expansion has been utilized. Expanding this result into series form produces,

$$P_{33}(z) = 1 - \frac{9}{8}(1 + \frac{7}{8}z + (\frac{7}{8})^2z^2 + (\frac{7}{8})^3z^3 + \dots) \quad (2.64)$$

$$+ \frac{1}{8}(1 - \frac{1}{8}z + (\frac{1}{8})^2z^2 - (\frac{1}{8})^3z^3 + \dots)$$

From Eq. (2.64), the cumulative distribution function of the process described by the system shown in Figure 2.17a can be obtained by inspection.

$$p_{33}(k) = 1 - \frac{9}{8}(\frac{7}{8})^k + \frac{1}{8}(-\frac{1}{8})^k \quad (2.65)$$

Notice from the equation as well as the diagram that $p_{33}(k) = 0$ for $k = 0, 1$ and that $p_{33}(k) \rightarrow 1$ as $k \rightarrow \infty$.

2.7 Absorbing Markov Chains

The following section exemplifies a method to evaluate the performance of lock-detectors. Lock-detectors indicate when a synchronization scheme is in/out of lock. The time required for this indication directly affects the performance (time) to acquire the code. The behavior of lock detectors can be modeled accurately by the use of Markov Chains.

A stochastic process X_n taking on values in a countable set is called a Markov chain with stationary transition probabilities if and only if

$$P[X_{n+1} = j | X_n = i ; A] = P[X_{n+1} = j | X_n = i] \quad (2.66)$$

where A is any other set of values for X_k for $k = 1$ to $n - 1$. Since the equation represents a one-step transition, it can be written as

$$p_{ij} = P[X_{n+1} = j | X_n = i] \quad (2.67)$$

Notice that the transition probability, p_{ij} , is not time dependent, meaning Eq. (2.67) holds for all n . Also, the initial state of the system must be specified. In this case, assume that the system is known to start in some fixed state, say $X_0 = i$, then

$$p_i = P[X_0 = i] = 1 \quad (2.68)$$

and

$$p_j = P[X_0 = j] = 0 \quad \text{for } j \neq i \quad (2.69)$$

Returning to the transition probability in Eq. (2.67), it can be noticed that $p_{ij} \geq 0$ for all i, j and $\sum_j p_{ij} = 1$ for all i . In fact, it is these restrictions which must be satisfied in order for p_{ij} to be the 1-step transition probabilities of a stationary Markov Chain. In order to explicitly show that the transition probability is for 1 time step, it will be denoted as $p_{ij}^{(1)} = p_{ij}$ and for an n -step transition,

$$p_{ij}^{(n)} = P[X_n = j | X_0 = i] \quad (2.70)$$

Obviously $n \geq 1$ so that

$$\begin{aligned} p_{ij}^{(n)} &= \sum_k p_{ik} p_{kj}^{(n-1)} \\ &= \sum_k p_{ik}^{(n-1)} p_{kj} \end{aligned} \quad (2.71)$$

where $p_{ij}^{(0)} = \delta_{ij}$ (δ_{ij} is the Kronecker delta).

The different states of the Markov chain can be classified into two distinct categories, transient and recurrent states. Transient states, as the name indicates, are only temporary in the sense that eventually the system will forever leave these states. The latter, recurrent states, are the absorbing states of the system. In other words, once these recurrent states are reached, the system does not leave from them. These ideas are clarified in the following example.

Assume a 4-state Markov Chain as in Figure 2.18. The transition probabilities, p_{ij} , can be put into matrix form as follows:

$$m = \begin{bmatrix} q & p & 0 & 0 \\ q & 0 & p & 0 \\ 0 & q & 0 & p \\ 0 & 0 & 0 & 1 \end{bmatrix} \quad (2.72)$$

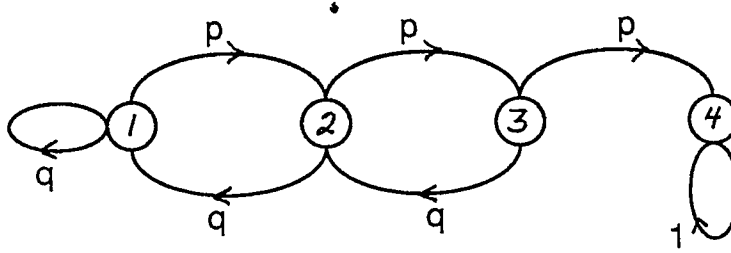


Figure 2.18 A 4-state absorbing Markov Chain

Notice for both the transition matrix as well as the state transition diagram that state 4 is an absorbing state. Assume that $P[X_1 = 1] = 1$, meaning that the state 1 is the starting point, then from Eq. (2.72),

$$p_{11} = q \quad p_{12} = p \quad p_{13} = 0 \quad p_{14} = 0 \quad (2.73)$$

It is also desirable to find the 2-step, 3-step and k-step transition probabilities of the system. Qualitatively, the 2-step transition probability can be found by

describing the various scenarios. Since the system starts in state X_1 , after 1 unit of time the system is in state 1 or 2 with probability q, p respectively. After the 2nd unit of time if the system was in state 1 then the probability of remaining there is q and if it was in state 2, the probability of returning to state 1 is q . So, $p_{11}^{(2)} = q \cdot q + p \cdot q$. This 2-step transition probability could have been calculated by squaring M as follows:

$$p_{ij}^{(2)} = m^2 = \begin{bmatrix} q & p & 0 & 0 \\ q & 0 & p & 0 \\ 0 & q & 0 & p \\ 0 & 0 & 0 & 1 \end{bmatrix} \begin{bmatrix} q & p & 0 & 0 \\ q & 0 & p & 0 \\ 0 & q & 0 & p \\ 0 & 0 & 0 & 1 \end{bmatrix} = \begin{bmatrix} q & pq & p^2 & 0 \\ q^2 & 2pq & 0 & p^2 \\ q^2 & 0 & pq & p \\ 0 & 0 & 0 & 1 \end{bmatrix} \quad (2.74)$$

This can similarly be repeated for any number of steps. In the next section, the mean time to reach the absorbing state will be calculated.

2.7.1 Mean Time to Absorption

In order to utilize the power of matrices, it is necessary to put the transition matrix into canonical form. The canonical matrix can be partitioned into four submatrices. The upper-left matrix is the grouping of the persistent states and is therefore by definition an identity matrix. It also follows that the upper right matrix will be the zero matrix. The lower-left matrix indicates the transition probability from a transient to an absorbing state and finally the lower-right matrix indicates the transient transitional probabilities. Consider the 4-state Markov chain described earlier,

$$[p_{ij}] = \begin{bmatrix} q & p & 0 & 0 \\ q & 0 & p & 0 \\ 0 & q & 0 & p \\ 0 & 0 & 0 & 1 \end{bmatrix} \quad (2.75)$$

would be rewritten as

$$[p_{ij}]^* = \begin{bmatrix} 1 & 0 & 0 & 0 \\ 0 & q & p & 0 \\ 0 & q & 0 & p \\ p & 0 & q & 0 \end{bmatrix} \quad (2.76)$$

In order to make this example more tractable, let $p = 7/8$ and $q = 1/8$. Substituting these values into Eq. (2.76),

$$[p_{ij}]^* = \begin{bmatrix} 1 & 0 & 0 & 0 \\ 0 & 1/8 & 7/8 & 0 \\ 0 & 1/8 & 0 & 7/8 \\ 7/8 & 0 & 1/8 & 0 \end{bmatrix} \quad (2.77)$$

From [6], the fundamental matrix, N , can be found as follows:

$$N = [I - Q]^{-1}$$

where Q is the lower-right matrix of the canonical matrix discussed above and $N = \{n_{ij}\}$ represents the number of steps spent in state j starting from state i (before being absorbed). From Eq. (2.77),

$$Q = \begin{bmatrix} 1/8 & 7/8 & 0 \\ 1/8 & 0 & 7/8 \\ 0 & 1/8 & 0 \end{bmatrix} \quad (2.79)$$

substituting into Eq. (2.78) and with some matrix calculations,

$$N = \begin{bmatrix} \frac{456}{7^3} & \frac{64}{7^2} & \frac{8}{7} \\ \frac{64}{7^3} & \frac{64}{7^2} & \frac{8}{7} \\ \frac{8}{7^3} & \frac{8}{7^2} & \frac{8}{7} \end{bmatrix} \quad (2.80)$$

From this matrix (Eq. 2.80), assuming unity dwell times, the mean number of times spent in state 1 starting in state 1 is $456/7^3$ before being absorbed. Similarly for state 2 starting from state 1 is $64/7^2$ and state 3 is $8/7$. Using this information, the number of time units spent in transient states before being absorbed is found to be (approximately) 3.77 by adding the elements of the first row. The usefulness and motivation for the absorption time is discussed in the next chapter. Here, it suffices to say that it aids in giving a measure of the overall performance of the system.

Having found the mean time in a transient state, the obvious question that follows is: What is the variance? In [6], a theorem for the variance of an equal dwell system is presented and a corollary to that is

$$\sigma_i^2 = 2N[T]QNT + NT_{i,2} - (NT)_{i,2} \quad (2.81)$$

where σ_i^2 represents the variance of the mean time to be absorbed starting in state i , $T_{i,2}$ and $(NT)_{i,2}$ represent the squaring of each element in the corresponding vector and $[T]$ is a matrix representing the T vector (elements of the vector are along the main diagonal of the matrix and zeroes elsewhere). Continuing with the example,

$$\sigma_1^2 = \begin{bmatrix} 15.45 \\ 15.27 \\ 12.46 \end{bmatrix} \quad (2.82)$$

The methods described in this and previous sections will be used in the next chapter to understand, evaluate and predict the performance of two different acquisition schemes.

Chapter 3

Direct Sequence PN Code Acquisition Schemes

In this chapter single and double-dwell schemes are evaluated and results compared. Although the single-dwell scheme is advantageous from a hardware complexity point of view, it may be desirable to invest in the more elaborate double dwell scheme in order to improve system performance.

The single-dwell acquisition scheme, shown in Fig. 3.1, was first analyzed by Holmes and Chen [7] where an expression for the mean and variance of the time to acquire the code was derived. This was done using the generating function that is first found from the signal flow diagram. In fact, DiCarlo and Weber [1] continued with the analysis and found the cumulative distribution function (CDF) of the number of steps to acquire the received PN code.

DiCarlo and Weber [10] worked with the results of Holmes and Chen and extended the results for a general multiple-dwell scheme. They present a generalized solution for the mean number of steps to acquire and an approximation for the variance. Perhaps due to the unwieldy nature of the expressions and the general nature of their presentation, an expression for the CDF is not derived. In order to make the results tractable, a double-dwell scheme is presented and analyzed in the latter part of this chapter and an approximate probability distribution function (PDF) is derived for the case of the double-dwell.

The performance results of both schemes are compared in Chapter 4 where the analysis of the preceding chapters is summarized and the marked improvement of the double dwell over the single dwell acquisition system is shown.

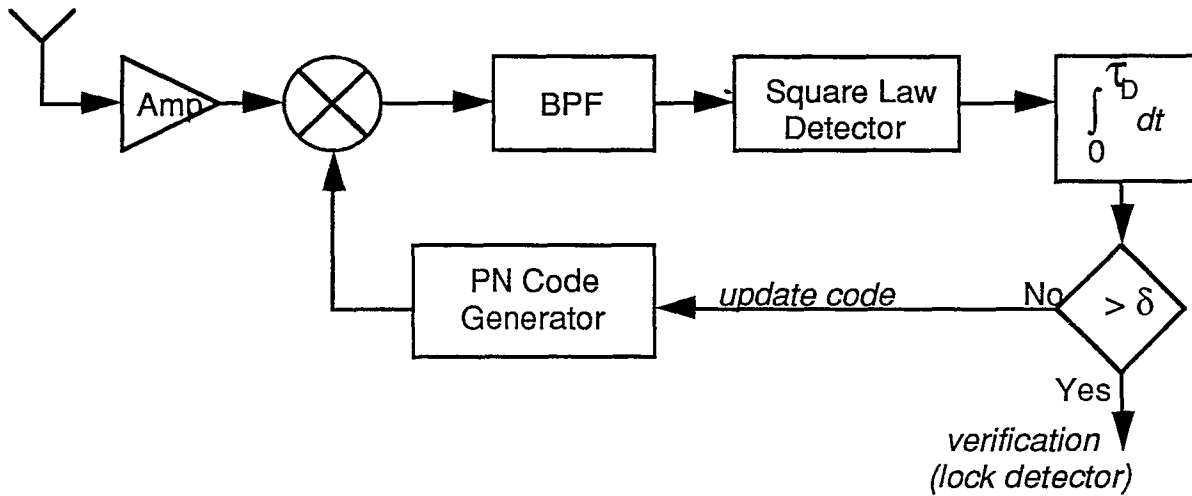


Figure 3.1 Block diagram of a single-dwell PN code acquisition system.

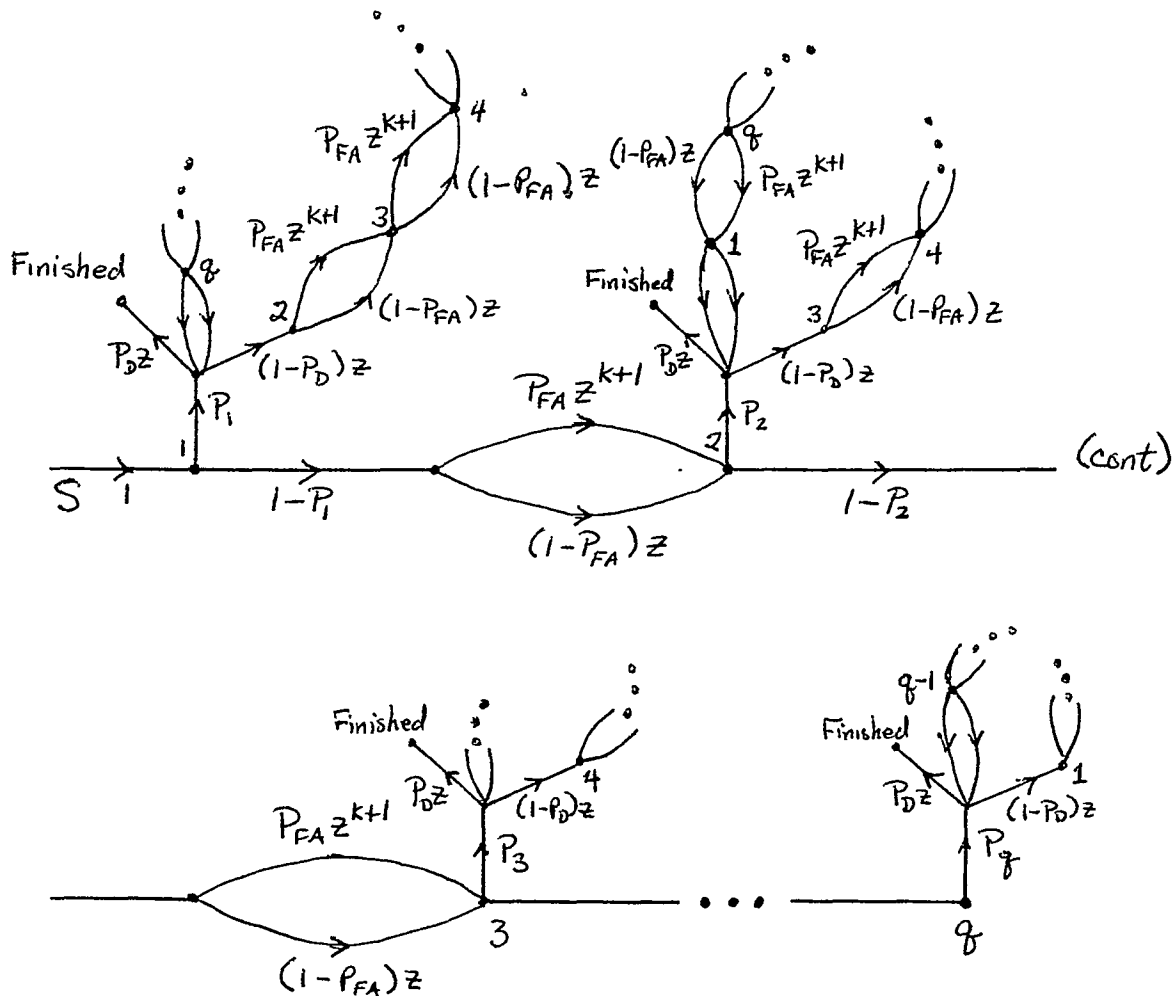


Figure 3.2 Signal Flow equivalent of a single-dwell PN code acquisition process.

3.1.1. Single-Dwell Model Description

Consider the PN acquisition system shown in Fig. 3.1. It can be seen that the system is a single-dwell (integration) type whose output is either above or below a certain threshold. There are four different situations that can occur during normal operation of the acquisition system. Assuming the correct cell is being tested, the output of the integrator at the end of the dwell time should be above the threshold. However, due to timing error and noise the integrator output at the end of the dwell time could be below the threshold resulting in a missed detection. The probability of this missed detection occurring is $1 - P_D$ where P_D is the probability of detection. It is also possible that when an incorrect cell is being searched the acquisition circuit can detect a false hit. This false alarm probability is P_{fa} and the probability of correctly dismissing the cell is $1 - P_{fa}$.

In order to understand the acquisition process quantitatively, refer to the equivalent signal flow diagram in Fig. 3.2. In the analysis, the cells are numbered from 1 to q where q is the number of dwells and not necessarily the code length (i.e. if there are two dwells per code chip then the number of chips is $q/2$). Recall

$$P_k = \frac{1}{q - k + 1} \quad (3.1)$$

where P_k is the probability that the k^{th} cell is a hit given that cells 1 thru $k - 1$ were misses (assuming uniform *a priori* distribution of the correct cell to be $1/q$).

Starting from node 1 in the signal-flow graph, the *a priori* probability of the correct cell being evaluated is $P_1 = 1/q$. Assuming the first cell is correct, moving upwards in the graph, the cell will be detected with probability P_D . This detection process requires one unit of dwell time so it is represented as $P_D z$. Once this branch is traversed, the acquisition process is complete. If, after traversing branch P_1 , the cell is not detected then the system will move to node 2 where one of two events may occur. This second (incorrect) cell may be dismissed after one unit of dwell, $(1 - P_{fa})z$, or it may be incorrectly detected as a hit in which case an additional K units of dwell time will be required to detect the false alarm. An explanation of why

K units of dwell time are attributed to the false-lock detection process is given in the next section. After reaching node 3, the process is repeated until the system returns to the correct cell. Again, the system will “acquire” the signal with probability P_D .

If the first cell is assumed incorrect, the system would move along the branch labelled $1 - P_1$ and again one of two events would occur. The system could dismiss the first cell with probability $1 - P_{fa}$ but this dismissal would require the evaluation (a single-dwell) of the cell, consuming one unit of time, hence the branch labelled $(1 - P_{fa})z$. It is also possible, with probability P_{fa} , that the system falsely detects a hit and this false detection would require one unit and the detection of the false alarm another K units, hence the branch $P_{fa}z^{K+1}$. This falso alarm penalty is discussed in the next section. Upon reaching node 2, the system would again move in a horizontal direction until the correct cell is reached and only then move upwards in the signal-flow diagram of Fig. 3.2.

3.1.2. Analysis of Single Dwell Acquisition

In order to derive the transfer function of the single-flow graph in Fig. 3.2, it is helpful to first reduce the different sections individually. In Fig. 3.3, the “loops” have to be simplified by addition of the branches entering the nodes and are relabelled with

$$A(z) = P_{fa}z^{K+1} + (1 - P_{fa})z \quad (3.2)$$

From Fig. 3.3 it can be noticed that the “loops” are basically feedback loops. Armed with the signal-flow theory presented in the previous chapter, the simplification finally results in Fig. 3.4 where

$$B_i(z) = \frac{P_i P_D z}{1 - (1 - P_D)z A^{q-1}(z)} \quad (3.3)$$

and

$$C_i(z) = (1 - P_i)A(z) \quad (3.4)$$

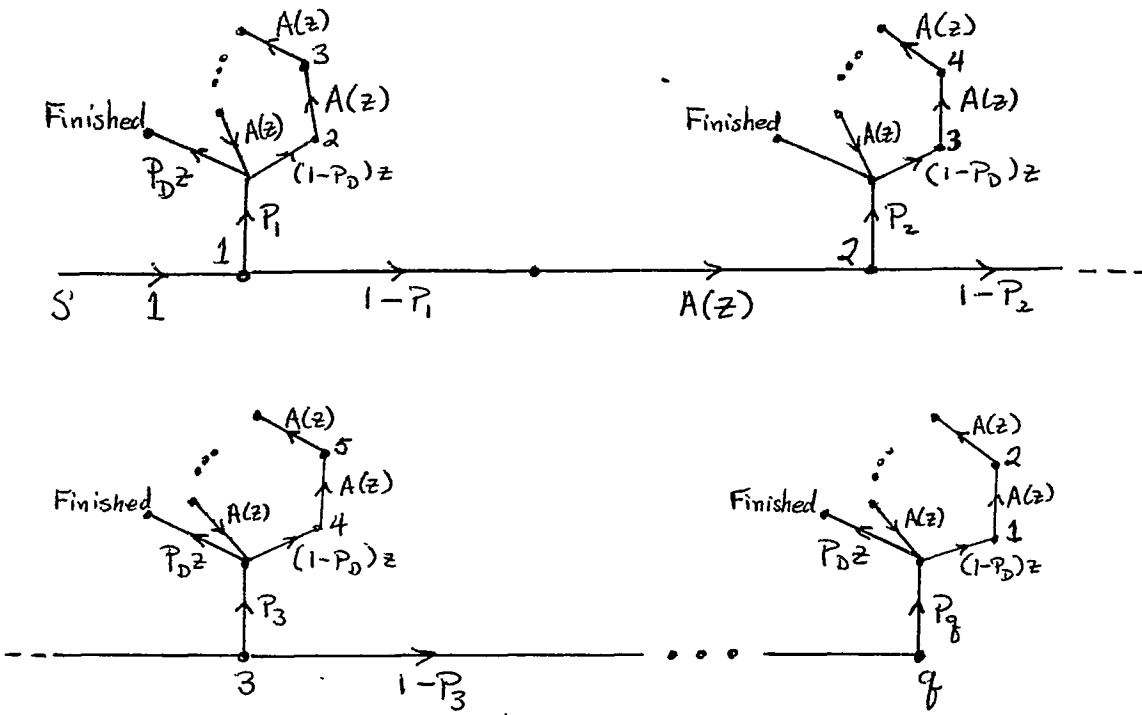


Figure 3.3 Partially reduced single-dwell signal flow graph.

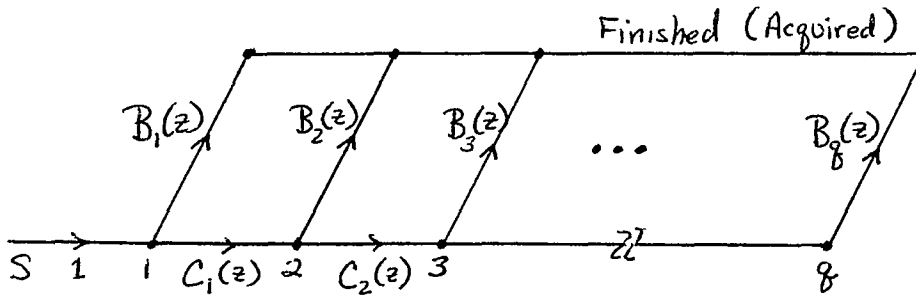


Figure 3.4 Reduced single-dwell signal flow graph.

The following notation
is used in the above figures:

$$A(z) = P_{fa} z^{k+1} + (1-P_{fa})z$$

$$B_i(z) = \frac{P_i P_D z}{1 - (1-P_D)z A^{q-1}(z)}$$

$$C_i(z) = (1-P_i)A(z)$$

From Fig. 3.4, the generating function, otherwise known as the transfer function can be found by inspection to be

$$P(z) = B_1(z) + C_1(z)B_2(z) + C_1(z)C_2(z)B_3(z) + \dots \\ \dots + C_1(z)C_2(z)\dots C_{q-1}(z)B_q(z) \quad (3.5)$$

This can be simplified by using Eqs. (3.3) and (3.4) as follows:

$$P(z) = \frac{P_D z}{1 - (1 - P_D)z A^{q-1}(z)} [P_1 + (1 - P_1)A(z)P_2 + (1 - P_1)(1 - P_2)A^2(z)P_3 + \dots \\ \dots + (1 - P_1)(1 - P_2)\dots(1 - P_{q-1})A^{q-1}(z)] \quad (3.6)$$

Using Eq. (3.1) directly in this expression yields

$$P(z) = \frac{P_D z}{1 - (1 - P_D)z A^{q-1}(z)} \left[\frac{1}{q} + \frac{q-1}{q} A(z) \cdot \frac{1}{q-1} + \frac{q-1}{q} \cdot \frac{q-2}{q-1} \cdot \frac{1}{q-2} A^2(z) + \dots \right. \\ \left. \dots + \frac{q-1}{q} \cdot \frac{q-2}{q-1} \dots \frac{2}{3} \cdot \frac{1}{2} A^{q-1}(z) \right] \quad (3.7)$$

When this is reduced, a common factor of $1/q$ remains so the series can be rewritten as

$$P(z) = \frac{P_D z/q}{1 - (1 - P_D)z A^{q-1}(z)} \sum_{i=0}^{q-1} A^i(z) \quad (3.8)$$

This represents the generating function of the acquisition system and from this equation the mean acquisition time can be derived (as explained in the previous chapter). In this case, since $P(1) = 1$, taking the natural logarithm first will yield the same results. Therefore,

$$\bar{T} = \frac{\partial}{\partial z} \ln P(z) \Big|_{z=1} \quad (3.9)$$

substituting Eq. (3.8) into Eq. (3.9) yields

$$\bar{T} = \frac{\partial}{\partial z} \left[\ln \frac{P_D z/q}{1 - (1 - P_D)z A^{q-1}(z)} + \ln \left(\sum_{i=0}^{q-1} A^i(z) \right) \right] \quad (3.10)$$

The first term of this equation is differentiated and when evaluated at $z = 1$ yields,

$$1 + \frac{1 - P_D}{P_D} [1 + (q-1)(1 + KP_{fa})] \quad (1^{st} \text{ term}) \quad (3.11a)$$

and the second term can also easily be reduced by using the fact that $A^i(z)|_{z=1} = 1$ for all i yields,

$$\frac{(q-1)(1+KP_{fa})}{2} \quad (2^{nd} \text{ term}) \quad (3.11b)$$

combining these terms and simplifying yields the result

$$\bar{T} = \frac{2 + (2 - P_D)(q-1)(1+KP_{fa})}{2P_D} \tau_D \quad (3.12)$$

This result was first derived by Holmes and Chen [7] and later confirmed by DiCarlo and Weber [10]. Notice that the mean time to acquisition has been written in terms of the unit dwell time, τ_D . This has been done so that the result is completely in terms of the system's parameters.

Notice that Eq. (3.12) can be checked for certain conditions; assume $P_D = 1$ and $P_{fa} = 0$ (ideal) then an acquisition time of

$$\bar{T} = \frac{q+1}{2} \tau_D \quad (3.13)$$

which is correct when the *a priori* probability distribution is $1/q$. Under normal circumstances, $q \gg 1$ and Eq. (3.12) can be approximated by

$$\bar{T} = \frac{(2 - P_D)(1 + KP_{fa})q}{2P_D} \tau_D \quad (3.14)$$

The variance of the acquisition time can also be found with the use of Eq. (2.54). Again, since $P(z)|_{z=1} = 1$, the variance is reduced to

$$\sigma_{T_{\text{acq}}}^2 = \left[\frac{\partial^2}{\partial z^2} \ln(P(z)) + \frac{\partial}{\partial z} \ln P(z) \right]_{z=1} = \frac{\partial^2}{\partial z^2} \ln(P(z)) + \bar{T} \quad (3.15)$$

The first term of Eq. (3.15) can be evaluated in the same manner as done for the mean and is shown in [7] which results in

$$\begin{aligned} \sigma_{T_{\text{acq}}}^2 \approx & \left[(1 + KP_{fa})^2 q^2 \left(\frac{1}{12} - \frac{1}{P_D} + \frac{1}{P_D^2} \right) + 6qK(K+1)P_{fa} \cdot 2P_D(1 - P_D) \right. \\ & \left. + 6q(1 + KP_{fa})(4 - 2P_D - P_D^2) + \frac{1 - P_D}{P_D^2} \right] \cdot \tau_D^2 \end{aligned} \quad (3.16)$$

where $q \gg 1$ has been assumed. In Eq. (3.16), the first term is dominant if

$K(K+1)P_{fa} \ll q$ hence

$$\sigma_{T_{acq}}^2 \approx (1 + KP_{fa})^2 q^2 \left(\frac{1}{12} - \frac{1}{P_D} + \frac{1}{P_D^2} \right) \tau_D^2 \quad (3.17)$$

This can also be checked for the ideal case where $P_{fa} = 0$ and $P_d = 1$,

$$\sigma_{T_{acq}}^2 \approx \frac{q^2 \tau_D^2}{12} \quad (3.18)$$

which is the variance of a random variable with uniform distribution.

Having found both the mean and the variance of the time for acquisition, it would be desirable to find the actual probability distribution function so that the probability of acquiring the signal by a certain time can be calculated. This performance criteria was the motivation of DiCarlo and Weber [10] and the results are derived here and it is shown that the mean time [7] can be derived from this probability distribution function.

Recall the generating function, $P(z)$, from Eq. (3.8). If it is possible to write the equation in the form of

$$P(z) = \sum_{j=0}^{\infty} p_j z^j \quad (3.19)$$

then it is possible to extract the probability distribution function of successful acquisition which is just the coefficient of z^j . With this in mind, from Eq. (3.8),

$$P(z) = \frac{P_D z / q}{1 - (1 - P_D)z A^{q-1}(z)} \sum_{i=0}^{q-1} A^i(z) \quad (3.20)$$

where $A(z) = P_{fa} z^{K+1} + (1 - P_{fa})z$. Using the series expansion,

$$\frac{1}{1 - (1 - P_D)z A^{q-1}(z)} = \sum_{j=0}^{\infty} [(1 - P_D)z A^{q-1}(z)]^j \quad (3.21)$$

and also recall that $A(z)$ is of the form

$$A(z) = (x + y) \quad (3.22)$$

where $x = P_{fa} z^{K+1}$ and $y = (1 - P_{fa})z$. From this,

$$A^i(z) = (x + y)^i = \sum_{h=0}^i \binom{i}{h} x^h y^{i-h} \quad (3.23)$$

Substitution of Eq. (3.21) into (3.20) yields

$$P(z) = \frac{P_D z}{q} \sum_{j=0}^{\infty} \sum_{i=0}^{q-1} (1 - P_D)^j z^j A^{j(q-1)}(z) A^i(z) \quad (3.24)$$

In Eq. (3.24), $A^{j(q-1)}(z) \cdot A^i(z) = A^{j(q-1)+i}(z)$ and this can be rewritten using Eq. (3.23) which results in

$$P(z) = \frac{P_D z}{q} \sum_{j=0}^{\infty} \sum_{i=0}^{q-1} \sum_{h=0}^{j(q-1)+i} (1 - P_D)^j z^j \cdot \binom{j(q-1)+i}{h} (P_{fa} z^{K+1})^h ((1 - P_{fa})z)^{j(q-1)+i-h} \quad (3.25)$$

Equation (3.25) can be simplified by combining like terms,

$$P(z) = \frac{P_D}{q} \sum_{j=0}^{\infty} \sum_{i=0}^{q-1} \sum_{h=0}^{j(q-1)+i} (1 - P_D)^j P_{fa}^h \cdot (1 - P_{fa})^{j(q-1)+i-h} \binom{j(q-1)+i}{h} z^{jq+i+hK+1} \quad (3.26)$$

In Eq. (3.26), the indices j , i , and h can be understood by noticing their effect on the exponent of z . The outermost index, j , represents the number of times the entire q cells were unsuccessfully searched. If $j = 0$ then it is the first pass and $j = 1$ implies that no successful synchronization occurred on the first pass, etc. The middle index, i , represents the cell number being checked during the j^{th} pass. Finally, the innermost index, h , from the exponent of z , indicates the number of false alarms.

From this point, DiCarlo and Weber [10] assume that the system is to synchronize during the first pass (by the q^{th} cell) in order to justify setting $j = 0$. This assumption is consistent with the fact that multiple passes will yield unacceptable acquisition times. This is quite accurate when P_D is close to 1, which reduces Eq. (3.26) to

$$P(z) = \frac{P_D}{q} \sum_{i=0}^{q-1} \sum_{h=0}^i \binom{i}{h} P_{fa}^h (1 - P_{fa})^{i-h} z^{i+hK+1} \quad (3.27)$$

It is also reasonable to assume that the penalty for false-lock^{is} to be less than the number of cells to be searched ($K < q$); otherwise the occurrence of even one false alarm would yield unacceptably long acquisition times. In this case, there are distinct ranges in which the exponent, r , can fall. The exponent, r , is the integral number of unit dwells which represents a particular moment in time (e.g. $r = 1$ implies $i = 1$ but $r = K + 1$ ^{could imply $i = K + 1$} or $h = 1$ and $i = 1$). The only way that a signal detection (otherwise known as a hit) can occur in the first range, $1 \leq r \leq K$, is if no false alarms occur ($h = 0$). In the second region, $K + 1 \leq r \leq 2K$, there are two possibilities. It may be that $h = 0$ and $K + 1 \leq i \leq 2K$ which implies no false alarms, or $h = 1$ and $1 \leq i \leq K$ which indicates one false alarm. Similarly, in the third region there are three possibilities: 0, 1 or 2 false alarms. These regions can be defined up to q (since $j = 0$ was established earlier). The generating function will now be analyzed quantitatively starting with the region

$$1 \leq r \leq K$$

$$P(z) = \frac{P_D}{q} \sum_{i=0}^{K-1} (1 - P_{fa})^i z^{i+1} \quad (3.28)$$

where direct substitution into Eq. (3.27) has been applied. Similarly, for the second region,

$$K + 1 \leq r \leq 2K$$

$$P(z) = \frac{P_D}{q} \left[\sum_{i=K}^{2K-1} (1 - P_{fa})^i z^{i+1} + \sum_{i=0}^{K-1} \binom{i}{1} P_{fa} (1 - P_{fa})^i z^{i+K+1} \right] \quad i = 0, h = 0, 1 \quad (3.29)$$

From Eq. (3.19), it is seen that the probability distribution function of a hit at the j^{th} cell is just the coefficient of the term z^j . So, once Eqs. (3.28) and (3.29) are rewritten, they will yield the probability coefficients p_j . Rewriting Eq. (3.28),

$$P(z) = \frac{P_D}{q} \sum_{i=1}^K \frac{P_D}{q} (1 - P_{fa})^{i-1} z^i \quad (3.30)$$

so

$$p_j = \frac{P_D}{q} (1 - P_{fa})^{j-1} \quad (3.31)$$

and for $0 \leq j < K$ Eq. (3.29) becomes,

$$P(z) = \frac{P_D}{q} \sum_{i=K}^{2K-1} \left[(1 - P_{fa})^{i-1} + \binom{i-1-k}{1} P_{fa}(1 - P_{fa})^{i-1-(K+1)} U[i-1-(K+1)] \right] z^i \quad (3.32)$$

where the second term has been multiplied by a step function so that Eq. (3.29) could be written in such a way that p_j is readily identified to be [1],

$$p_j = \frac{P_D}{q} \left[(1 - P_{fa})^{j-1} + \binom{j-1-k}{1} P_{fa}(1 - P_{fa})^{j-1-(K+1)} U[j-1-(K+1)] \right] \quad (3.33)$$

for $K < j < 2K$. In Eq. (3.33) the first and second terms represent the possibilities of zero and one false alarm, respectively. Since the purpose of this section is to create a framework for the double-dwell system, for $j > 2K$, the reader is referred to [1].

3.2. Lock-Detector Analysis

Lock detectors are used in PN acquisition systems to verify code synchronization and to dismiss false-locks. The lock detector requires a finite amount of time to accomplish these tasks. In fact, the mean time to indicate false-lock is the “penalty” assigned to a false alarm. Figure 3.5 represents the detection process of a single-dwell acquisition scheme. In order to modify the system into a double-dwell scheme, another integrator after the comparator would be needed to retest under a longer dwell (of course, another decision device) as in Fig. 3.7. A three-count lock-detector is shown in Fig. 3.6 and can be used in both the single and double-dwell systems. Therefore the following analysis is independent of which acquisition scheme is used and the results hold for both the single and double-dwell schemes which are discussed in this chapter.

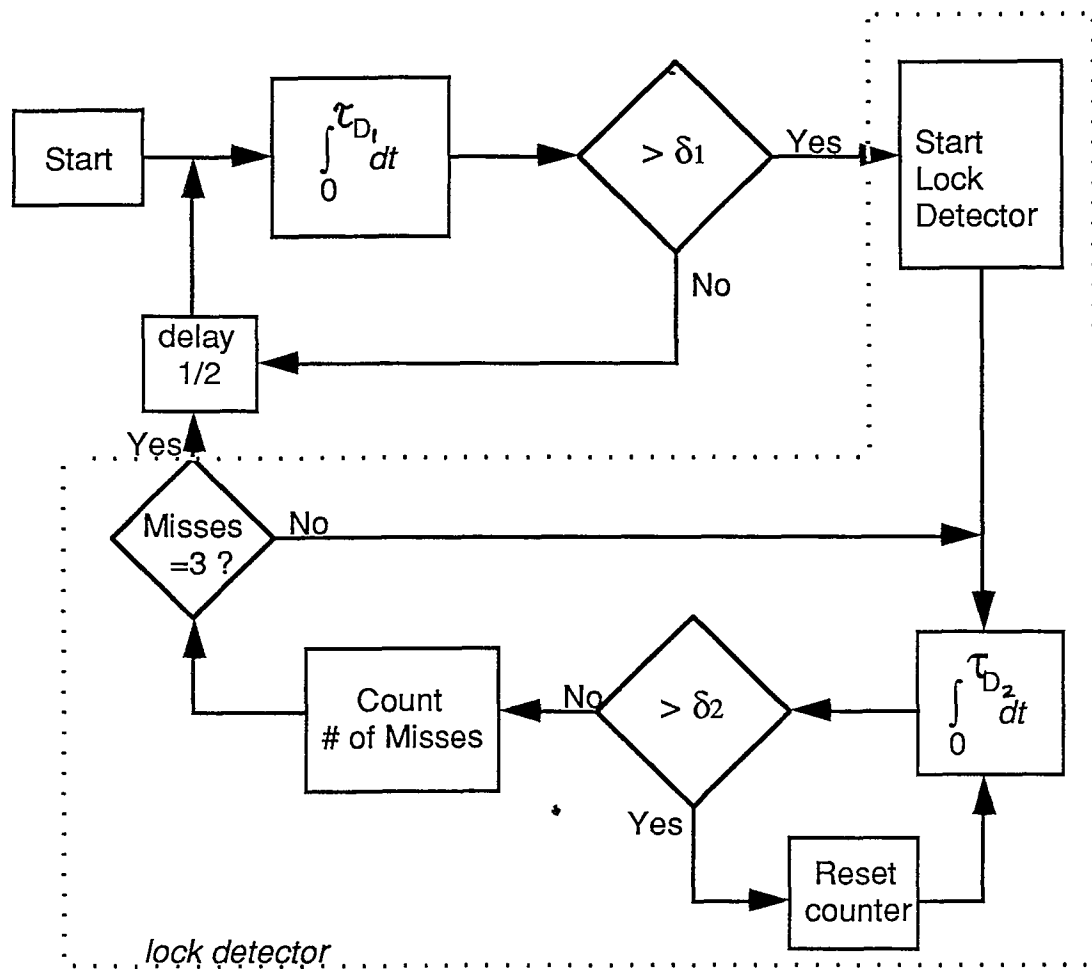


Figure 3.5 Single-dwell detection process

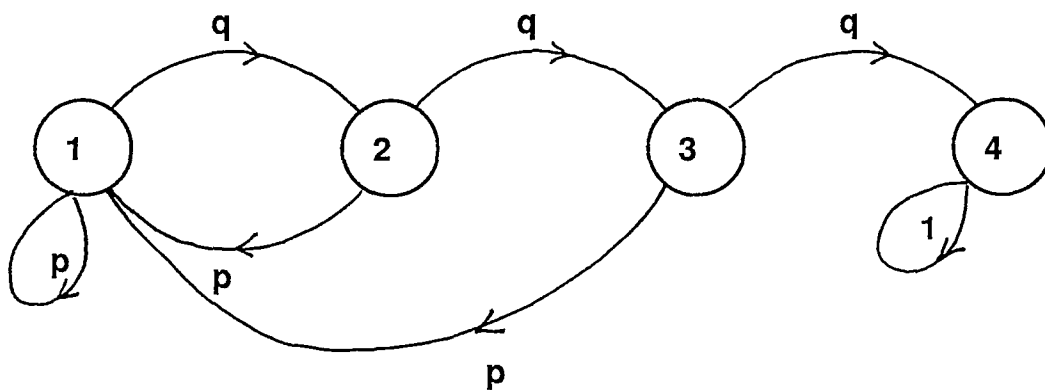


Figure 3.6 3-count lock detector state transition diagram

3.2.1. Evaluation of the Penalty: K

In order to analyze Fig. 3.6, the theory of absorbing Markov chains, as discussed in the previous chapter, will be used to help find the mean time to detect false-lock, \bar{T}_{fl} . The state transition matrix is given by

$$[p_{ij}] = \begin{bmatrix} p & q & 0 & 0 \\ p & 0 & q & 0 \\ p & 0 & 0 & q \\ 0 & 0 & 0 & 1 \end{bmatrix} \quad (3.35)$$

where $p = \text{Prob}(\text{hit})$ and $q = \text{Prob}(\text{no hit})$ in the false-lock mode. As in Eq. (2.76), this can be rewritten in canonical form as

$$[p_{ij}]^* = \begin{bmatrix} 1 & 0 & 0 & 0 \\ 0 & p & q & 0 \\ 0 & p & 0 & q \\ q & p & 0 & 0 \end{bmatrix} \quad (3.36)$$

Using Eq. (2.78), the fundamental matrix is

$$N = \begin{bmatrix} \frac{q^2 + pq + p}{q^3} & \frac{1}{q^2} & \frac{1}{q} \\ \frac{p(1+q)}{q^3} & \frac{1}{q^2} & \frac{1}{q} \\ \frac{p}{q} + \frac{p(p+pq)}{q^3} & \frac{p}{q^2} & \frac{1}{q} \end{bmatrix} \quad (3.37)$$

To find the mean time spent in states 1, 2 and 3 before being absorbed, simply add the elements of the first row and this yields the result which has been proven by Holmes [6] in general to be

$$\bar{T}_{\text{fl}} = \frac{1 + q + q^2 + \dots + q^{n-1}}{q^n} \tau_{\text{LDD}} \quad (3.38)$$

where an n -count detector with equal (lock-detector) dwells of duration τ_{LDD} is assumed. In the case of Eq. (3.37),

$$\bar{T}_{\text{fl}} = \frac{1 + q + q^2}{q^3} \tau_{\text{LDD}} \quad (3.39)$$

In order to make the analysis more tractable, it is assumed that τ_{LDD} is a multiple of τ_D (τ_{D2} for double-dwell) so that it is possible to rewrite Eq. (3.39) as

$$\bar{T}_R = K\tau_D \quad (3.40)$$

where $K = (1 + q + q^2)/q^3$ and τ_{LDD} has been (reasonably) assumed. Equation (3.40) indicates that a false alarm will cause the system acquisition process to be delayed by K dwells which is referred to as the false-alarm penalty. This “penalty” is one of the parameters needed in order to calculate the mean acquisition time of the code acquisition system.

3.3. Double-Dwell Acquisition Scheme

Having evaluated the performance of a single-dwell system, it is noticed that there is not much freedom inherent in the system. The natural extension of a single-dwell scheme is the double-dwell. The purpose of this section is to find the generating function of the double-dwell system which will lead to the mean and variance of the acquisition time. As in the single-dwell system, it is much desired to find the probability distribution function. With this motivation, a close approximation is derived and the results are presented and compared with known special cases.

3.3.1. Model Description

Implementation of a double-dwell acquisition system is shown in Fig. 3.7. The analysis of this system will follow that of the single-dwell, in which the generating function is first found. This section will only deal with the description of the system and the analysis follows in the next section.

Notice that Fig. 3.7 is only a generalization of the single-dwell system. The first integration period is to search (τ_{D1}) and quickly dismiss incorrect code phases. Once the first threshold, δ_1 , is exceeded, the second integration is used to insure that the code phase is in fact in synchronization with the received code. The system can be

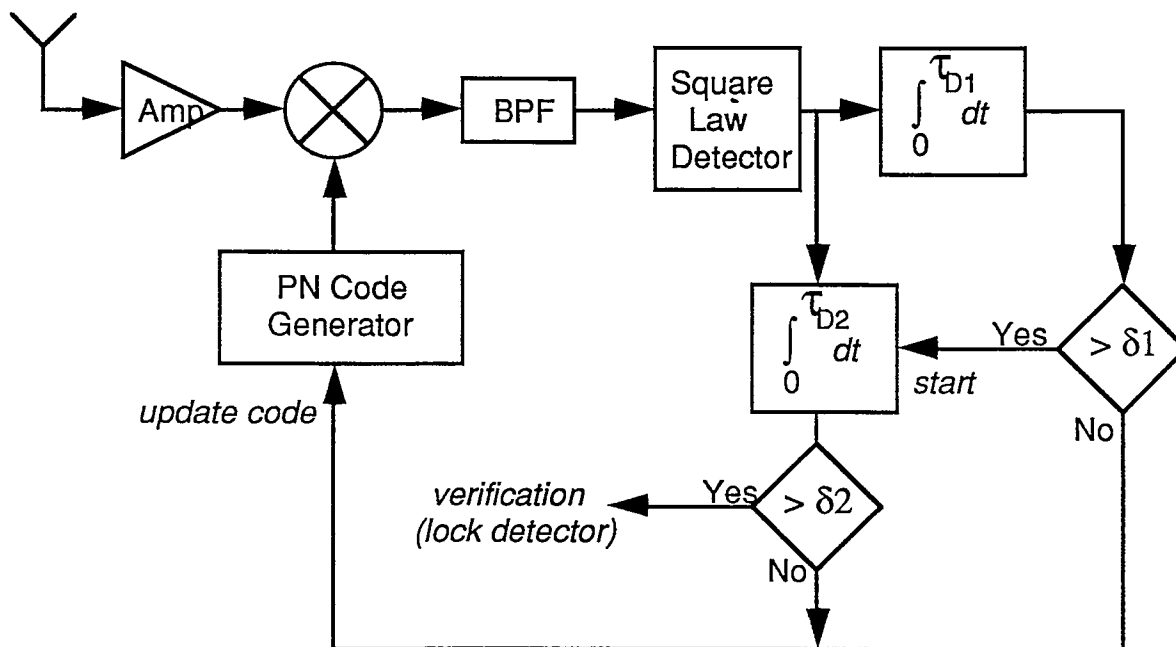


Figure 3.7 Double-dwell PN code acquisition system.

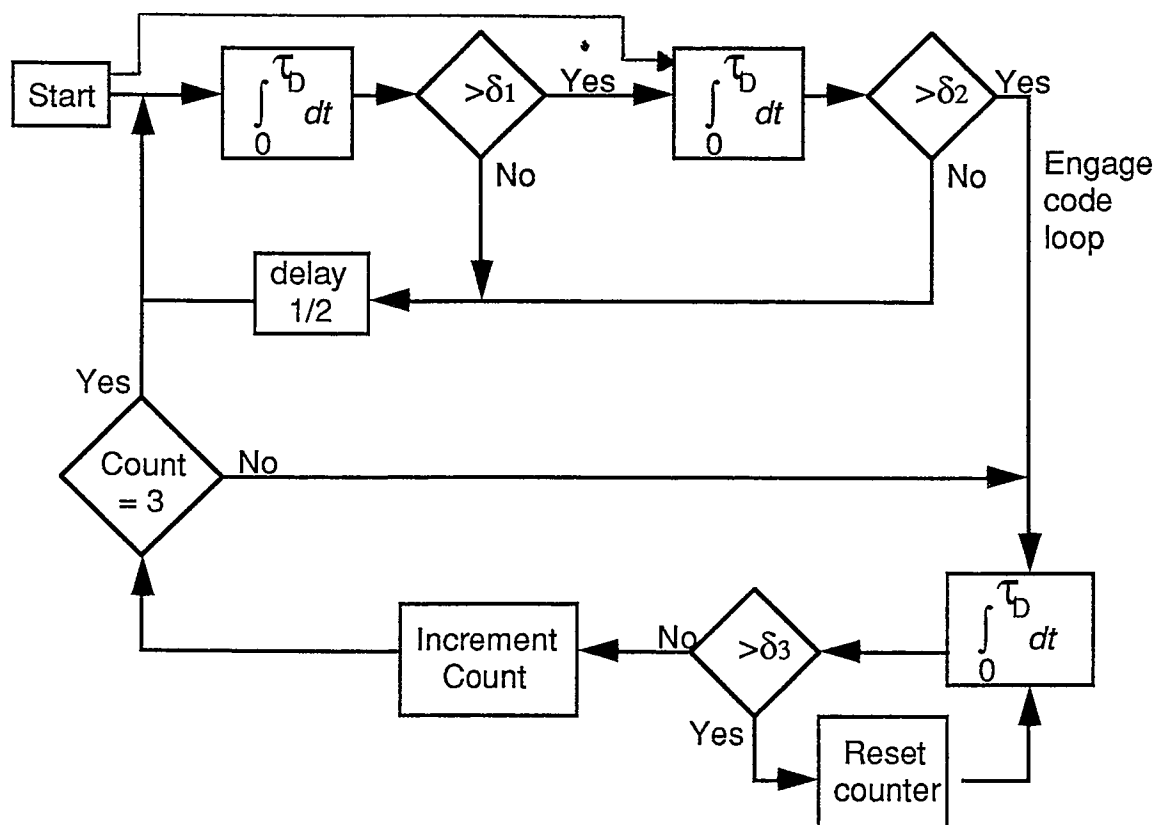


Figure 3.8 Double-dwell detection/verification process

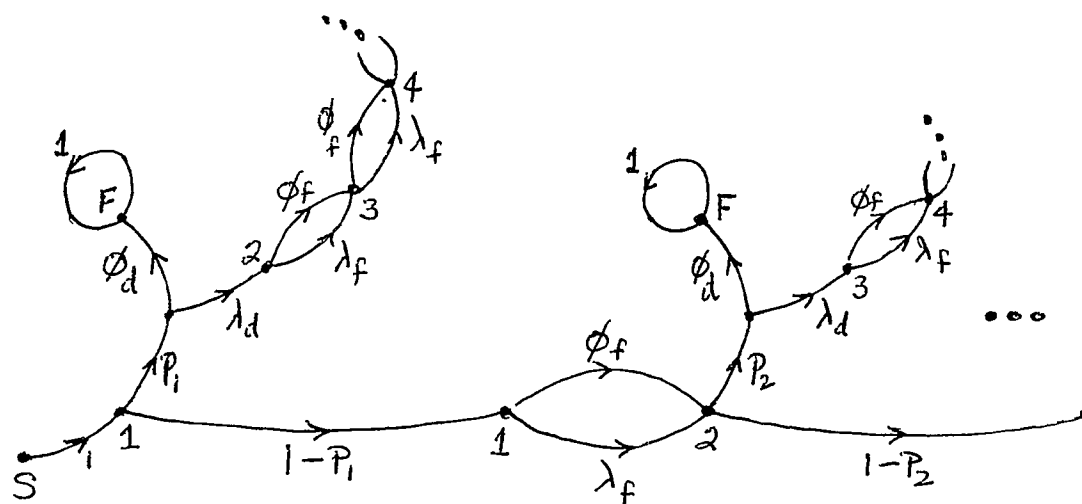
correctly thought of as a two-stage process. In the first stage, if there is a remote possibility that the correct cell is being searched then the system will advance to the second stage. This implies that both the probability of false alarm and probability of detection are high for the first stage. It is possible however that some of the local code phases will have a low correlation with the received code so that they may be (quickly) dismissed by the first stage. If the system does reach the second stage, a more accurate (longer) dwell is needed so that the false alarm probability is reduced and at the same time the probability of detection is kept high. If the second integrator output is above the prespecified threshold then the system will advance to the verification mode, shown in Fig. 3.8.

The verification mode is the operation of the lock-detector which is discussed in the previous section. The resulting idea is that the detector can be modelled as a system where it requires K units (average) of dwell (τ_{D_2}) to detect a false alarm. These K units of dwell are termed the false alarm penalty and is used in the evaluation of the double-dwell system discussed here.

3.3.2. System Analysis

In order to derive the acquisition statistics of the double-dwell scheme, it is necessary to find the generating function. As for the single-dwell case, a signal-flow diagram must first be constructed to model the double-dwell process.

The double-dwell signal-flow graph is just an extension of Fig. 3.2 which represents the single-dwell system. In Fig. 3.9 the double-dwell process is represented in a signal-flow diagram where the dwell times τ_1 and τ_2 are represented by z_1 and z_2 respectively. In Fig. 3.9a, assuming the first cell is correct, then the system will traverse the first vertical path, P_1 . If the system locks onto the correct cell, then the branch ϕ_d will be traversed. It is also possible that this correct cell is missed, which is represented by λ_d . This miss could occur if the first dwell is below the threshold $(1 - P_{d_1})z_1$ or it is possible that the miss occurs on the second dwell, $P_{d_1}z_1(1 - P_{d_2})z_2$.



(a)

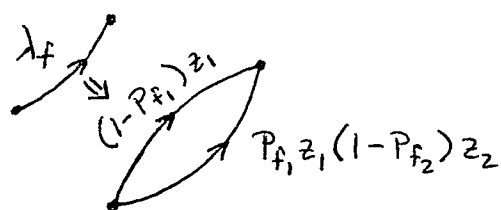
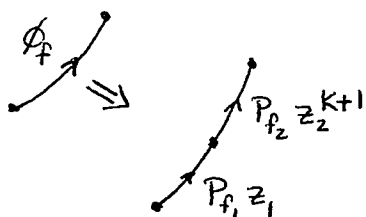
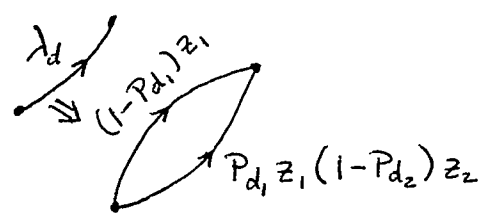
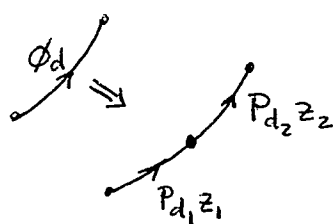


Figure 3.9 Signal-Flow representation of the double-dwell scheme.

If the second, rather than the first, cell is assumed to be correct the system would travel along the branch labelled $1 - P_1$ and at this point the system should dismiss the first cell. A relatively quick dismissal can occur, represented as λ_f , in two ways: If the first threshold is not exceeded or if the second threshold is not exceeded. It is also possible that a false alarm situation arises due to both the first and second dwells exceeding their thresholds and this is represented by ϕ_f . Notice that a penalty of K units has been assigned to the second false alarm. The justification of this penalty is discussed in the previous section. Once the second node is reached, the same procedure is repeated until the correct cell is detected (represented by node F) and only then will the system properly lock.

As in the case of the single-dwell process, it is desirable to write the transfer/generating function in the form of Eq. (3.20) so that it will be possible to eventually find the probability distribution function of the acquisition process.

From Fig. 3.9, using the same techniques as in Section 3.1, it is possible to reduce the generating function to

$$P(z) = \frac{\phi_d/q}{1 - \lambda_d A^{q-1}(z)} \sum_{i=0}^{q-1} A^i(z) \quad (3.41)$$

where $A(z) = \lambda_f + \phi_f$. In the next section, Eq. (3.41) is derived from a diagram that is equivalent with Fig. 3.9 but leads to the generating function. Notice the similarity of Eq. (3.41) with (3.8). In order to make the analysis similar to the single-dwell, it is necessary to define the detection probabilities as

$$\phi_d = P_{d_1} z_1 P_{d_2} z_2 \quad (3.42)$$

$$\lambda_d = (1 - P_{d_1}) z_1 + P_{d_1} z_1 (1 - P_{d_2}) z_2 \quad (3.43)$$

$$\phi_f = P_{f_1} z_1 P_{f_2} z_2^{K+1} \quad (3.44)$$

$$\lambda_f = (1 - P_{f_1}) z_1 + P_{f_1} z_1 (1 - P_{f_2}) z_2 \quad (3.45)$$

where ϕ_d and λ_d are the probabilities of detection and missed detection, respectively (including the time weighting). Similarly, ϕ_f and λ_f are the probabilities of a false

alarm and correct dismissal, respectively (including the time penalty for false lock). In order to reduce the system to a single-dwell, set $P_{d_1} = P_{f_1} = 1$ and absorb the delay z_1 (dwell-time) into the second dwell z_2 . This would cause the system's performance to be equivalent to the single-dwell system. Returning to the double-dwell case, it is desirable to find the mean time to acquisition.

3.3.3. Acquisition Parameters

For the double-dwell system, the acquisition time, T_a , is given by

$$T_a = x_1\tau_1 + x_2\tau_2 \quad (3.46)$$

where x_1 and x_2 represent the number of dwells of duration τ_1 and τ_2 , respectively. In order to find the mean acquisition time, we take the ensemble average

$$E[T_a] = E[x_1]E[\tau_1] + E[x_2]E[\tau_2] \quad (3.47)$$

Since the dwell times are fixed, Eq. (3.47) reduces to

$$E[T_a] = E[x_1]\tau_1 + E[x_2]\tau_2 \quad (3.48)$$

In order to find $E[x_1]$, the method presented in Section 3.1.2 will be followed closely. Equation (3.9) can be generalized to apply in this case as

$$E[x_1] = \left. \frac{\partial P(z)}{\partial z_1} \right|_{z=1} \quad (3.49a)$$

and

$$E[x_2] = \left. \frac{\partial P(z)}{\partial z_2} \right|_{z=1} \quad (3.49b)$$

Substituting Eq. (3.41) into Eq. (3.49a),

$$\begin{aligned} E[x_1] &= \frac{\partial}{\partial z_1} \left[\frac{\phi_d/q}{1 - \lambda_d A^{q-1}(z)} \right] \sum_{i=0}^{q-1} A^i(z) \bigg|_{z=1} + \frac{\phi_d/q}{1 - \lambda_d A^{q-1}(z)} \sum_{i=0}^{q-1} i A^{i-1}(z) \frac{\partial A(z)}{\partial z_1} \bigg|_{z=1} \\ &= \frac{\partial}{\partial z_1} \left[\frac{\phi_d}{1 - \lambda_d A^{q-1}(z)} \right] \bigg|_{z=1} + \frac{q-1}{2} \frac{\partial A(z)}{\partial z_1} \bigg|_{z=1} \end{aligned} \quad (3.50)$$

Applying the results of [10] for the double dwell case yields,

$$E[x_1] = \frac{(q-1)(1-P_{d_1}P_{d_2})}{P_{d_1}P_{d_2}} + \frac{q-1}{2} \quad (3.51)$$

Similarly, using Eq. (3.41) in (3.49b) yields,

$$E[x_2] = \frac{\partial}{\partial z_2} \left[\frac{\phi_d/q}{1 - \lambda_d A^{q-1}(z)} \sum_{i=0}^{q-1} A^i(z) \right] \Big|_{z=1} + \frac{\phi_d/q}{1 - \lambda_d A^{q-1}(z)} \sum_{i=0}^{q-1} i A^{i-1}(z) \frac{\partial}{\partial z_2} A(z) \Big|_{z=1} \quad (3.52)$$

Again, using the results of [10] we note that the first term of Eq. (3.52) becomes

$$\frac{P_{d_1} + (q-1)(1-P_{d_1}P_{d_2})[P_{f_1} + KP_{f_1}P_{f_2}]}{P_{d_1}P_{d_2}} \quad (3.53a)$$

and the second term simplifies as follows:

$$\frac{\phi_d/q}{1 - \lambda_d A^{q-1}(z)} \sum_{i=0}^{q-1} i A^{i-1}(z) \frac{\partial}{\partial z_2} A(z) \Big|_{z=1} = \frac{q-1}{2} \frac{\partial A(z)}{\partial z_2} \Big|_{z=1} = \frac{q-1}{2} (P_{f_1} + KP_{f_1}P_{f_2}) \quad (3.53b)$$

Substituting (3.53) into Eq. (3.52) yields

$$E[x_2] = \frac{P_{d_1} + (q-1)(1-P_{d_1}P_{d_2})[P_{f_1} + KP_{f_1}P_{f_2}]}{P_{d_1}P_{d_2}} + \frac{q-1}{2} (P_{f_1} + KP_{f_1}P_{f_2}) \quad (3.54)$$

Therefore, combining the results of Eq. (3.51) and (3.54), the mean time for acquisition, assuming $q \gg 1$, is

$$\begin{aligned} E[T_a] &\approx \left\{ \frac{q(1-P_{d_1}P_{d_2})}{P_{d_1}P_{d_2}} + \frac{q}{2} \right\} \tau_1 \\ &\quad + \left\{ \frac{P_{d_1} + q(1-P_{d_1}P_{d_2})(P_{f_1} + KP_{f_1}P_{f_2})}{P_{d_1}P_{d_2}} + \frac{q}{2} (P_{f_1} + KP_{f_1}P_{f_2}) \right\} \tau_2 \\ &= \frac{q(2-P_{d_1}P_{d_2})}{2P_{d_1}P_{d_2}} \tau_1 + \frac{2P_{d_1} + q(2-P_{d_1}P_{d_2})(P_{f_1} + KP_{f_1}P_{f_2})}{2P_{d_1}P_{d_2}} \tau_2 \end{aligned} \quad (3.55)$$

Having found the mean time to acquisition for the double-dwell case, an approximation of the variance of acquisition time can be found using the following definition [13],

$$\sigma^2 \triangleq E[T_a^2] - E^2[T_a] \quad (3.56)$$

However, since $P(z)|_{z=1} = 1$, the following [7] formula also applies

$$\sigma^2 = \frac{\partial^2}{\partial z_1^2} P(z) \Big|_{z=1} \tau_1^2 + 2 \frac{\partial^2}{\partial z_1 \partial z_2} P(z) \Big|_{z=1} \tau_1 \tau_2 + \frac{\partial^2}{\partial z_2^2} P(z) \Big|_{z=1} \tau_2^2 + E[T_a] - E^2[T_a] \quad (3.57)$$

Using the sufficient condition [10],

$$q \gg \max \left[\frac{P_{f2} K(K+1)}{(1-P_d)} \right] \quad (3.58)$$

it is found that

$$\frac{\partial^2 P(z)}{\partial z_1^2} \Big|_{z=1} \approx q^2 \left(\frac{1}{3} + \frac{2}{P_d^2} - \frac{2}{P_d} \right) \quad (3.59a)$$

$$\frac{\partial^2 P(z)}{\partial z_1 \partial z_2} \Big|_{z=1} \approx q^2 \left(\frac{1}{3} + \frac{2}{P_d^2} - \frac{2}{P_d} \right) (K P_f + P_{f1}) \quad (3.59b)$$

$$\frac{\partial^2 P(z)}{\partial z_2^2} \Big|_{z=1} \approx q^2 \left(\frac{1}{3} + \frac{2}{P_d^2} - \frac{2}{P_d} \right) (K P_f + P_{f1})^2 \quad (3.59c)$$

Substituting Eqs. (3.55) and (3.59) into Eq. (3.57) yields

$$\begin{aligned} \sigma^2 \approx & q^2 \left(\frac{1}{3} + \frac{2}{P_d^2} - \frac{2}{P_d} \right) \tau_1^2 \\ & + 2q^2 \left(\frac{1}{3} + \frac{2}{P_d^2} - \frac{2}{P_d} \right) (K P_f + P_{f1}) \tau_1 \tau_2 \\ & + q^2 \left(\frac{1}{3} + \frac{2}{P_d^2} - \frac{2}{P_d} \right) (K P_f + P_{f1})^2 \tau_2^2 \\ & + E[T_a] \\ & - E^2[T_a] \end{aligned} \quad (3.60)$$

where $E[T_a]$ is given by Eq. (3.55). This simplifies to

$$\sigma^2 \approx q^2 \left(\frac{1}{3} + \frac{2}{P_d^2} - \frac{2}{P_d} \right) [\tau_1 + (K P_f + P_{f1}) \tau_2]^2 \quad (3.61)$$

$- q^2 \left(\frac{2-P_d}{2P_d} \tau_1 + \frac{(2-P_d)(P_{f1}+K P_f)}{2P_d} \tau_2 \right)^2$

where only terms containing quadratic q were kept.

As done previously for the single-dwell acquisition system, it is desirable to find the probability distribution function. Once the pdf is found, the time required to achieve a specific level of certainty can be computed.

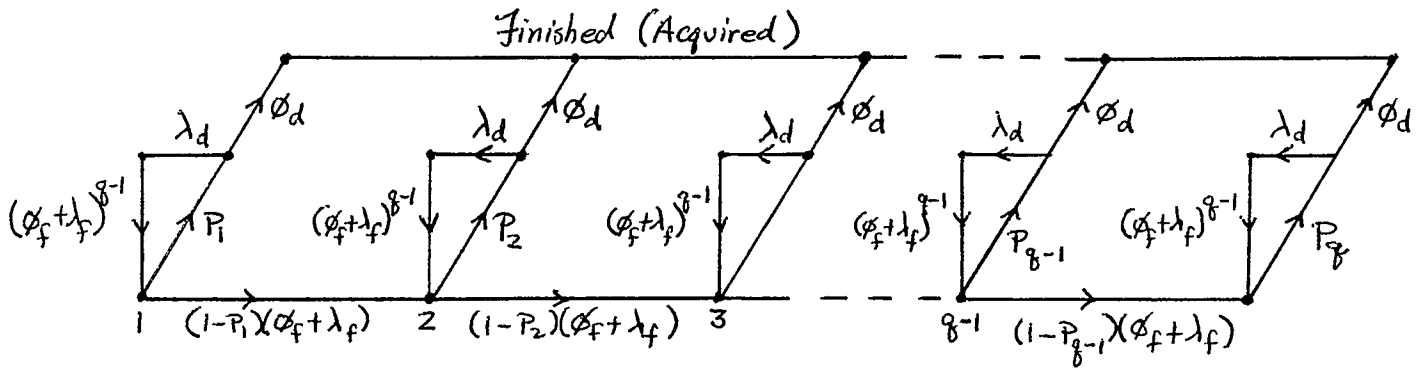


Figure 3.10 Partially reduced double-dwell signal flow graph

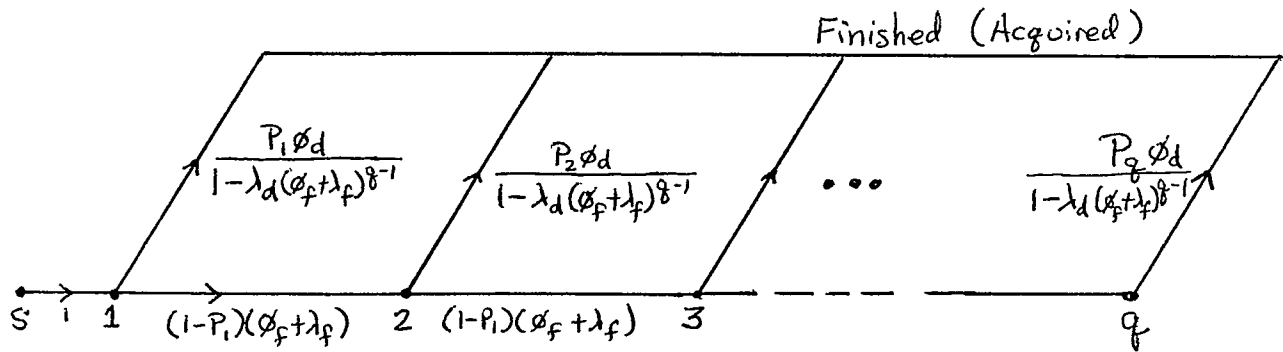


Figure 3.11 Reduced signal-flow graph for double-dwell acquisition scheme

The single-dwell can be viewed as a simplified version of the double-dwell scheme, hence the motivation for simplifying Fig. 3.9. Figure 3.10 is a straightforward combination of the branches on the flow graph, making use of the fact that all locked (finished) nodes are common. Upon eliminating the feedback loops, the result is Fig. 3.11.

From Fig. 3.11, the generating function, otherwise known as the transfer function is found (by inspection) to be:

$$\begin{aligned}
P(z) &= \frac{P_1 \phi_d}{1 - \lambda_d(\phi_f + \lambda_f)^{q-1}} + (1 - P_1)(\phi_f + \lambda_f) \frac{P_2 \phi_d}{1 - \lambda_d(\phi_f + \lambda_f)^{q-1}} \\
&\quad + (1 - P_1)(1 - P_2)(\phi_f + \lambda_f)^2 \frac{P_3 \phi_d}{1 - \lambda_d(\phi_f + \lambda_f)^{q-1}} + \dots \\
&\quad \dots + (1 - P_1)(1 - P_2) \dots (1 - P_{q-1})(\phi_f + \lambda_f)^{q-1} \frac{P_q \phi_d}{1 - \lambda_d(\phi_f + \lambda_f)^{q-1}} \\
&= \frac{\phi_d}{1 - \lambda_d(\phi_f + \lambda_f)^{q-1}} [P_1 + (1 - P_1)(\phi_f + \lambda_f)P_2 + \dots \\
&\quad \dots + (1 - P_1)(1 - P_2) \dots (1 - P_{q-1})(\phi_f + \lambda_f)^{q-1}]
\end{aligned} \tag{3.62}$$

Just as Eq. (3.7) was simplified and rewritten, the same is done with Eq. (3.62),

$$P(z) = \frac{\phi_d/q}{1 - \lambda_d(\phi_f + \lambda_f)^{q-1}} \sum_{i=0}^{q-1} (\phi_f + \lambda_f)^i \tag{3.63}$$

In order to find the approximate pdf from the generating function, Eqs. (3.23), (3.42)-(3.45) are employed below to make the equation more understandable from an applications point of view. It will then be possible to make approximations to arrive at a compact solution to the pdf for a double-dwell acquisition scheme.

$$\begin{aligned}
P(z) &= \frac{\phi_d/q}{1 - \lambda_d(\phi_f + \lambda_f)^{q-1}} \sum_{m=0}^{q-1} (\phi_f + \lambda_f)^m \\
&= \frac{\phi_d}{q} \sum_{j=0}^{\infty} [\lambda_d(\phi_f + \lambda_f)^{q-1}]^j \sum_{m=0}^{q-1} \sum_{h_1=0}^m \binom{m}{h_1} \phi_f^{h_1} \lambda_f^{m-h_1} \\
&= \frac{\phi_d}{q} \sum_{j=0}^{\infty} \{ \lambda_d(\phi_f + \lambda_f)^{q-1} \}^j \sum_{m=0}^{q-1} \sum_{h_1=0}^m \binom{m}{h_1} P_{f_1}^{h_1} P_{f_2}^{h_1} (z_1 z_2^{K+1})^{h_1}
\end{aligned}$$

$$\begin{aligned}
& \cdot \{(1 - P_{f_1})z_1 + P_{f_1}(1 - P_{f_2})z_1z_2\}^{m-h_1} \\
& = \frac{\phi_d}{q} \sum_{j=0}^{\infty} \left\{ \lambda_d(\phi_f + \lambda_f)^{q-1} \right\}^j \sum_{m=0}^{q-1} \sum_{h_1=0}^m \binom{m}{h_1} P_{f_1}^{h_1} P_{f_2}^{h_1} (z_1 z_2^{K+1})^{h_1} \\
& \quad \cdot \sum_{h_2=0}^{m-h_1} \binom{m-h_1}{h_2} \{(1 - P_{f_1})z_1\}^{h_2} \cdot \{P_{f_1}(1 - P_{f_2})z_1z_2\}^{m-h_1-h_2} \\
& = \frac{\phi_d}{q} \sum_{j=0}^{\infty} \left\{ \lambda_d(\phi_f + \lambda_f)^{q-1} \right\}^j \sum_{m=0}^{q-1} \sum_{h_1=0}^m \sum_{h_2=0}^{m-h_1} \binom{m}{h_1} \binom{m-h_1}{h_2} P_{f_1}^{h_1} P_{f_2}^{h_2} (1 - P_{f_1})^{h_2} \\
& \quad \cdot P_{f_1}^{m-h_1-h_2} (1 - P_{f_2})^{m-h_1-h_2} (z_1 z_2^{K+1})^{h_1} z_1^{h_2} (z_1 z_2)^{m-h_1-h_2} \\
& = \frac{\phi_d}{q} \sum_{j=0}^{\infty} \left\{ \lambda_d(\phi_f + \lambda_f)^{q-1} \right\}^j \sum_{m=0}^{q-1} \sum_{h_1=0}^m \sum_{h_2=0}^{m-h_1} \binom{m}{h_1} \binom{m-h_1}{h_2} P_{f_1}^{m-h_2} P_{f_2}^{h_1} (1 - P_{f_1})^{h_2} \\
& \quad \cdot (1 - P_{f_2})^{m-h_1-h_2} z_1^m z_2^{m+Kh_1-h_2} \\
& = \frac{P_{d_1} P_{d_2}}{q} \sum_{j=0}^{\infty} \left\{ [(1 - P_{d_1})z_1 + P_{d_1}(1 - P_{d_2})z_1z_2]^j \right. \\
& \quad \cdot [P_{f_1} P_{f_2} z_1 z_2^{K+1} + (1 - P_{f_1})z_1 + P_{f_1} z_1 (1 - P_{f_2})z_2]^{j(q-1)} \left. \right\} \\
& \quad \cdot \sum_{m=0}^{q-1} \sum_{h_1=0}^m \sum_{h_2=0}^{m-h_1} \binom{m}{h_1} \binom{m-h_1}{h_2} P_{f_1}^{m-h_2} P_{f_2}^{h_1} (1 - P_{f_1})^{h_2} \\
& \quad \cdot (1 - P_{f_2})^{m-h_1-h_2} z_1^{m+1} z_2^{m+Kh_1-h_2+1} \\
& = \frac{P_{d_1} P_{d_2}}{q} \sum_{j=0}^{\infty} \sum_{m=0}^{q-1} \sum_{h_1=0}^m \sum_{h_2=0}^{m-h_1} \sum_{i=0}^j \sum_{\ell=0}^{j(q-1)} \binom{j}{i} [(1 - P_{d_1})z_1]^i \cdot [P_{d_1}(1 - P_{d_2})z_1z_2]^{j-1} \\
& \quad \cdot \binom{j(q-1)}{\ell} [P_{f_1} P_{f_2} z_1 z_2^{K+1}]^{\ell} \cdot [(1 - P_{f_1})z_1 + P_{f_1} z_1 (1 - P_{f_2})z_2]^{j(q-1)-\ell} \\
& \quad \cdot \binom{m}{h_1} \binom{m-h_1}{h_2} P_{f_1}^{m-h_2} P_{f_2}^{h_1} (1 - P_{f_1})^{h_2} (1 - P_{f_2})^{m-h_1-h_2} z_1^{m+1} z_2^{m+Kh_1-h_2+1} (3.64)
\end{aligned}$$

Equation (3.64) is an explicit expansion of the generating function and will allow for reasonable assumptions to be made concerning the double dwell scheme. First, the equation must be rewritten with all z terms grouped together so that the effect

of the indices on the time can be understood.

$$\begin{aligned}
P(z) = & \frac{P_{d_1} P_{d_2}}{q} \sum_{j=0}^{\infty} \sum_{m=0}^{q-1} \sum_{h_1=0}^m \sum_{h_2=0}^{m-h_1} \sum_{i=0}^j \sum_{\ell=0}^{j(q-1)} \sum_{p=0}^{j(q-1)-\ell} \binom{j}{i} (1-P_{d_1})^i P_{d_1}^{j-i} (1-P_{d_2})^{j-i} \\
& \cdot \binom{j(q-1)}{i} P_{f_1}^{\ell} P_{f_2}^{\ell} \binom{j(q-1)-\ell}{p} (1-P_{f_1})^p P_{f_1}^{j(q-1)-\ell-p} (1-P_{f_2})^{j(q-1)-\ell-p} \\
& \cdot \binom{m}{h_1} \binom{m-h_1}{h_2} P_{f_1}^{m-h_2} P_{f_2}^{h_1} (1-P_{f_1})^{h_2} (1-P_{f_2})^{m-h_1-h_2} \\
& \cdot z_1^{jq+m+1} z_2^{jq-i+\ell K-p+m+Kh_1-h_2+1}
\end{aligned} \tag{3.65}$$

Equation (3.65) is similar to the generating function of the single-dwell which is represented by Eq. (3.26). In order to understand some of the indices of summation, it is useful to notice their effect on z_1 and z_2 . As in the single-dwell, the outermost index, j , represents the number of times the entire q cells were unsuccessfully searched. As an example, $j = 0$ implies it is the first pass and $j = 1$ means that no successful synchronization occurred on the first pass. Just as DiCarlo and Weber assumed the single-dwell system to synchronize during the first pass, the same is done for the double-dwell justifying $j = 0$. It is important to notice that $i = 0$ is forced because i ranges from 0 to j ; the same is also true for ℓ and p . Taking the above into account yields,

$$\begin{aligned}
P(z) = & \frac{P_{d_1} P_{d_2}}{q} \sum_{m=0}^{q-1} \sum_{h_1=0}^m \sum_{h_2=0}^{m-h_1} \binom{m}{h_1} \binom{m-h_1}{h_2} P_{f_1}^{m-h_2} P_{f_2}^{h_1} (1-P_{f_1})^{h_2} (1-P_{f_2})^{m-h_1-h_2} \\
& \cdot z_1^{m+1} \cdot z_2^{m+Kh_1-h_2+1}
\end{aligned} \tag{3.66}$$

The generating function is now analyzed starting with the first region,

For $1 \leq r \leq K$ ($h_1 = h_2 = 0$)

$$P(z) = \frac{P_{d_1} P_{d_2}}{q} \sum_{m=0}^{K-1} P_{f_1}^m (1-P_{f_2})^m z_1^{m+1} z_2^{m+1} = \frac{P_{d_1} P_{d_2}}{q} \sum_{m=1}^K P_{f_1}^{m-1} (1-P_{f_2})^{m-1} z_1^m z_2^m$$

Therefore, the pdf is,

$$P_j = \frac{P_{d_1} P_{d_2}}{q} P_{f_1}^{j-1} (1 - P_{f_2})^{j-1} \quad (3.67a)$$

For the second region, there are numerous cases. For the purpose of illustration, three different cases are shown.

For $K + 1 \leq r \leq 2K$

I. $h_1 = h_2 = 0$

$$P(z) = \sum_{m=K}^{2K-1} \frac{P_{d_1} P_{d_2}}{2} P_{f_1}^m (1 - P_{f_2})^m z_1^{m+1} z_2^{m+1} = \frac{P_{d_1} P_{d_2}}{q} \sum_{m=K+1}^{2K} P_{f_1}^{m-1} (1 - P_{f_2})^{m-1} z_1^m z_2^m$$

Therefore, the pdf is,

$$P_j = \frac{P_{d_1} P_{d_2}}{q} P_{f_1}^{j-1} (1 - P_{f_2})^{j-1} \quad (3.67b)$$

II. $h_1 = 1, h_2 = 0$

$$\begin{aligned} P(z) &= \frac{P_{d_1} P_{d_2}}{2} \sum_{m=0}^{K-1} m P_{f_1}^m P_{f_2} (1 - P_{f_2})^{m-1} z_1^{m+1} z_2^{m+K+1} \\ &= \frac{P_{d_1} P_{d_2}}{q} \sum_{m=1}^K (m-1) P_{f_1}^{m-1} P_{f_2} (1 - P_{f_2})^{m-2} z_1^m z_2^{m+K} \end{aligned}$$

Therefore, the pdf is,

$$P_j = \frac{P_{d_1} P_{d_2}}{q} P_{f_1}^{j-1} P_{f_2} (1 - P_{f_2})^{j-2} U[j-2] \quad (3.67c)$$

III. $h_1 = 1, h_2 = 1$

$$\begin{aligned} P(z) &= \frac{P_{d_1} P_{d_2}}{2} \sum_{m=0}^{K-1} m(m-1) P_{f_1}^{m-1} P_{f_2} (1 - P_{f_1}) (1 - P_{f_2})^{m-2} z_1^{m+1} z_2^{m+K} \\ &= \frac{P_{d_1} P_{d_2}}{q} \sum_{m=1}^K (m-1)(m-2) P_{f_1}^{m-2} P_{f_2} (1 - P_{f_1}) (1 - P_{f_2})^{m-3} z_1^m z_2^{m+K-1} \end{aligned}$$

Therefore, the pdf is,

$$P_j = \frac{P_{d_1} P_{d_2}}{q} P_{f_1}^{j-2} P_{f_2} (1 - P_{f_1}) (1 - P_{f_2})^{j-3} U[j-3] \quad (3.67d)$$

The above equations are examples to show the specific nature of different possibilities. It is for this reason only a small number of cases are shown and it should be noted for a particular case, all possibilities would have to be worked out.

Having found a general expression for the PDF of the double-dwell acquisition system, it is useful to compare the performance of the single and double-dwell acquisition schemes. This comparison and discussion about the advantages of each system is carried out in the next and final chapter.

Chapter 4 Conclusions

4.1 System Comparisons

In this final chapter, a comparison of the single and double dwell acquisition schemes is made. It is shown that a definite time advantage is gained by investing in the double-dwell acquisition system.

Eq. (3.14) and (3.17) represent the mean and variance of the time to acquire the PN sequence using a single dwell system. After normalization, these equations become

$$\bar{T}_{acq}/q\Delta = \frac{(2 - P_D)(1 + KP_{fa})}{2P_D} \tau_D/\Delta \quad (4.1)$$

$$\sigma_T/q\Delta = (1 + KP_{fa}) \sqrt{\frac{1}{12} - \frac{1}{P_D} + \frac{1}{P_D^2}} \tau_D/\Delta \quad (4.2)$$

Similarly, for the double dwell scheme, Eq. (3.55) and (3.61) represent the mean and variance, respectively. After normalization,

$$\bar{T}_{acq}/q\Delta = \frac{2 - P_D}{2P_D} \tau_1/\Delta + \frac{2 - P_D}{2P_D} P_{f1} (1 + KP_{f2}) \tau_2/\Delta \quad (4.3)$$

$$\sigma_T/q\Delta = \left[\left(\frac{1}{3} + \frac{2}{P_D^2} - \frac{2}{P_D} \right) (\tau_1 + (P_{f1} + KP_{f2}) \tau_2)^2 - \left(\frac{2 - P_D}{2P_D} \tau_1 + \frac{(2 - P_D)(P_{f1} + KP_{f2})}{2P_D} \tau_2 \right)^2 \right]^{1/2} / \Delta \quad (4.4)$$

Notice that in Eq. (4.3) if $\tau_1=0$ and $P_{fa} = 1$ then the equation is identical with the equation which represents the mean time to acquisition for the single dwell scheme.

Now, the results from the previous chapter will be utilized to assess the performance of the single and double dwell PN code acquisition schemes. In order to evaluate the two schemes, the following approximation for the false-alarm probability [10] is used

$$P_f \approx Q\left(\frac{\sqrt{\frac{\tau_D}{\Delta}}(SNR) - Q^{-1}(1 - P_D)\sqrt{2 + SNR}}{\sqrt{2 + 2(SNR)}}\right) \quad (4.5)$$

where $Q(x) = \frac{1}{\sqrt{2\pi}} \int_x^\infty e^{-\lambda^2/2} d\lambda$ is the area under the Gaussian tail.

In order to make a fair comparison between the two schemes, the signal to noise ratio (SNR) should be kept constant. In PN acquisition schemes, it is not rare for the SNR to be less than -10dB. For this comparison, SNR=-20 dB and a false alarm penalty of $K=10\tau_2$ is first assumed. For both the single and double dwell schemes, with this example, one may draw the incorrect conclusion that a minimization of the acquisition time can be achieved by arbitrarily increasing the false-alarm rate. This is shown incorrect by repeating the process with a penalty of $K=100\tau_2$. In Figure 4.2, an increase in mean acquisition time is shown by increasing the false alarm rate from $P_{fa}=10^{-2}$ to $P_{fa}=10^{-3}$.

Before comparing the two systems, it is useful to understand the method in which the parameters were calculated. In Table 4.1, the first entry, P_d is the desired detection probability. Recall in chapter 3, it is assumed that detection will occur on first pass. In order to be consistent with this, the detection probability must be very close or equal to 1. (For the purpose of system comparison, $P_d=0.99$ to $P_d=0.9999$). The second and third column entries vary from $P_{fa}=10^{-2}$ to $P_{fa}=10^{-4}$. The fourth and fifth columns are determined from the previous entries using Eq. (4.5). Notice that the dwell time

P_D	P_{f_1}	P_{f_2}	τ_1/Δ	τ_2/Δ	$\bar{T}_{acq}/q\Delta$	$\sigma_T/q\Delta$
0.99	1.00E-02	-	4451	-	2498	1497
0.99	1.00E-03	-	5987	-	3085	1849
0.99	1.00E-04	-	7453	-	3806	2282
0.99	1.00E-01	1.00E-01	2683	2683	1642	985
0.99	1.00E-01	1.00E-02	2683	4451	1618	917
0.99	1.00E-02	1.00E-02	4451	4451	2296	1300
0.999	1.00E-02	-	5983	-	3297	1911
0.999	1.00E-03	-	7746	-	3919	2272
0.999	1.00E-04	-	9402	-	4715	2878
0.999	1.00E-01	1.00E-01	3897	3897	2343	1430
0.999	1.00E-01	1.00E-02	3897	5983	2282	1318
0.999	1.00E-02	1.00E-02	5983	5983	3030	1747
0.9999	1.00E-02	-	7445	-	4095	2365
0.9999	1.00E-03	-	9398	-	4747	2742
0.9999	1.00E-04	-	11214	-	5614	3242
0.9999	1.00E-01	1.00E-01	5092	5092	3056	1869
0.9999	1.00E-01	1.00E-02	5092	7445	2956	1710
0.9999	1.00E-02	1.00E-02	7445	7445	3764	2174

Table 4.1 Single vs. Double Dwell Acquisition Parameters and Statistics ($K=10\tau_2$).

P_D	P_{f_1}	P_{f_2}	τ_1/Δ	τ_2/Δ	$\bar{T}_{acq}/q\Delta$	$\sigma_T/q\Delta$
0.99	1.00E-02	-	4451	-	4541	2723
0.99	1.00E-03	-	5987	-	3359	2014
0.99	1.00E-04	-	7453	-	3840	2302
0.99	1.00E-01	1.00E-01	2683	2683	2874	1723
0.99	1.00E-01	1.00E-02	2683	4451	1822	1031
0.99	1.00E-02	1.00E-02	4451	4451	2316	1311
0.999	1.00E-02	-	5983	-	5995	3475
0.999	1.00E-03	-	7746	-	4269	2474
0.999	1.00E-04	-	9402	-	4757	2904
0.999	1.00E-01	1.00E-01	3897	3897	4100	2503
0.999	1.00E-01	1.00E-02	3897	5983	2552	1470
0.999	1.00E-02	1.00E-02	5983	5983	3057	1763
0.9999	1.00E-02	-	7445	-	7446	4301
0.9999	1.00E-03	-	9398	-	5170	2986
0.9999	1.00E-04	-	11214	-	5664	3271
0.9999	1.00E-01	1.00E-01	5092	5092	5348	3270
0.9999	1.00E-01	1.00E-02	5092	7445	3291	1899
0.9999	1.00E-02	1.00E-02	7445	7445	3797	2193

Table 4.2 Single vs. Double Dwell Acquisition Parameters and Statistics ($K=100\tau_2$).

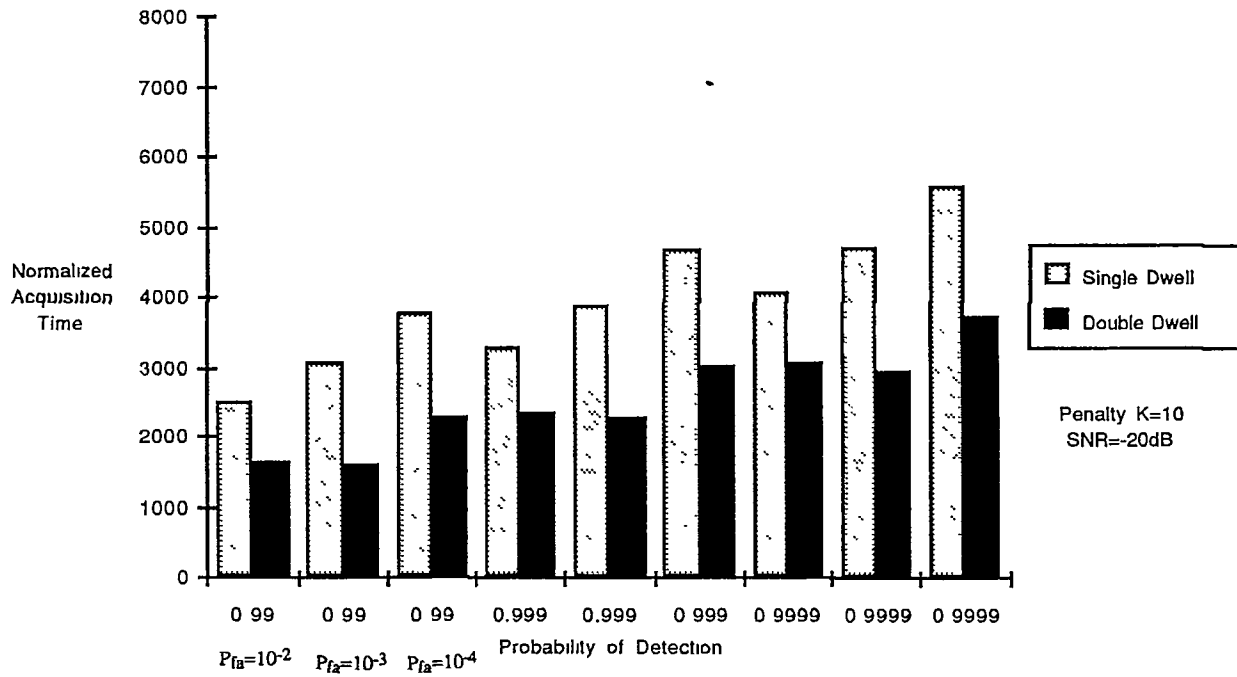


Figure 4.1 Mean Single vs. Double Dwell Acquisition Times ($K=10\tau_2$).

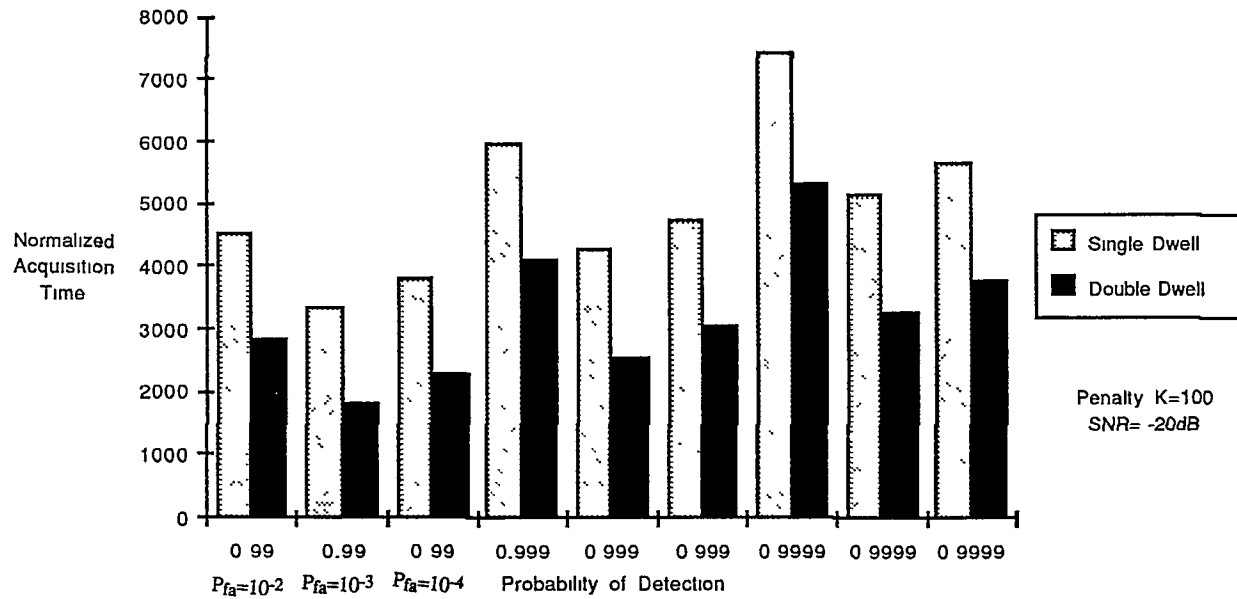


Figure 4.2 Mean Single vs. Double Dwell Acquisition Times ($K=100\tau_2$).

cannot be written explicitly in terms of P_{fa} and P_d . This inability is the reason that a computer is needed to numerically calculate the optimal value false alarm rate needed to obtain the optimal (minimum) acquisition time. Finally, the mean and variance columns are determined from the calculated data using Eq. (4.1-2) and (4.3-4) for the single and double dwell schemes, respectively. By changing the penalty for false-lock, Table 4.2 is generated. Armed with these tables, an understanding and comparison of the two systems is possible.

Referring to Fig. 4.1, notice three entries for the same probability of detection. These entries differ in the acceptable false alarm rate. The probability of false alarm, P_{fa} , for the first second and third entries is $P_{fa}=10^{-2}$, 10^{-3} , 10^{-4} , respectively. This method allows for the straight-forward comparison of different system configurations. The only parameter that is changed in Fig. 4.2 is the false-lock penalty, K . In this case, contrary to intuition, it is clearly more useful to design the double dwell system with $P_d=0.9999$ and $P_{fa}=10^{-4}$ than $P_d=0.9999$ and $P_{fa}=10^{-2}$, the former yielding an acquisition time of 71% of the latter. By reducing the number of penalties, which is now $K=100\tau_2$, the system is able to spend less time in false-locks thereby reducing the overall acquisition time.

It is apparent from Table 4.1-2 that the double dwell scheme requires an average of only 64% of the time required for acquisition using the single dwell scheme. This significant reduction in acquisition time is accompanied by a decrease in the variance as well. These performance improvements come at the expense of hardware complexity and depending on the application, the increase in capital may be justified.

Assuming the initial cost of the system is not the primary criteria on which system design is selected, it may be worthwhile to investigate a triple-dwell scheme. The analysis to find the system's statistics will directly follow the material presented in this work but will be quite tedious.

It is interesting to note, in addition to the reduced acquisition time, the double-dwell system lends itself to an adaptive process. Based on the percentage of false alarms in the first and second dwells, the system could vary the duration of the dwells thereby optimizing the system with respect to the false-alarm rate.

In conclusion, it is apparent that the double dwell acquisition scheme is clearly superior to the single dwell scheme in terms of the mean time to acquisition. This superiority comes at the expense of hardware complexity and cost. Since PN acquisition schemes are largely used for military communications, the increased cost is easily justified by the benefits of a fast acquisition system.

4.2 Recommendations for Future Work

It would be interesting to construct a detailed simulation model of the single and double dwell acquisition systems. With such a simulated system, the acquisition time could be determined for large numbers (a few thousand) of independent trial runs with random initial phases and additive noise. From this data, one could obtain an estimate of the mean, variance and pdf of the acquisition time. These values could be compared to the theoretical values to indicate the effect the assumptions had on the derivation of the results.

Appendix A

Recall Eq. (1.13) and notice that the mixer and ideal bandpass filter is a correlator. Taking $y_r(t)$ and correlating it with the “late” PN code, $c(t - \hat{T} - T_c/2)$,

$$y_L(t) = \sqrt{2P} d(t - T) E[c(t - T) c(t - \hat{T} - T_c/2)] \sin(\omega_0 t + \theta) + n_f(t) \quad (A.1)$$

where $n_f(t)$ is the bandpass filtered noise. We can rewrite Eq. (A.1) using the fact that

$$R_c(T - \hat{T} - T_c/2) = E[c(t - T) c(t - \hat{T} - T_c/2)] \quad (A.2)$$

yielding

$$y_L(t) = \sqrt{2P} d(t - T) R_c(T - \hat{T} - T_c/2) \sin(\omega_0 t + \theta) + n_f(t) \quad (A.3)$$

From this, it is possible to find e_ϵ^+ , one of the inputs to the summer, in Figure 1.4. Upon squaring Eq. (A.3) and only retaining terms that pass through the lowpass filter, yields

$$e_\epsilon^+ = P d^2(t - T) R_c^2(t - \hat{T} - T_c/2) + n_f^2(t) \quad (A.4)$$

and similarly for the early channel,

$$e_\epsilon^+ = P d^2(t - T) R_c^2(t - \hat{T} + T_c/2) + n_f'^2(t) \quad (A.5)$$

where we have denoted the noise term as $n_f'^2(t)$ to distinguish between the noise components of the different channels. Subtracting Eq. (A.5) from Eq. (A.4) yields the error signal,

$$\begin{aligned} e_\epsilon &= e_\epsilon^+ - e_\epsilon^- \\ &= P d^2(t - T) [R_c^2(t - \hat{T} + T_c/2) - R_c^2(t - \hat{T} - T_c/2)] \\ &\quad + n_f^2(t) - n_f'^2(t) \end{aligned} \quad (A.6)$$

using the fact that $d^2(t - T) = 1$ and letting $N(t) = n_f^2(t) - n_f'^2(t)$ simplifies the result to

$$e_\epsilon = P[R_c^2(t - \hat{T} - T_c/2) - R_c^2(t - \hat{T} + T_c/2)] + N(t) \quad (A.7)$$

For maximal length sequences, the autocorrelation difference in Eq. (A.7) can be simplified by using the autocorrelation function explicitly. The autocorrelation function of $c(t)$ is

$$R_c(\tau) = 1 - \frac{\tau}{T_c} \left(1 + \frac{1}{N}\right) \quad (A.8)$$

where N is the period of the sequence. Using Eq. (A.8), the error signal equation can be simplified by using the fact that $\epsilon = T - \hat{T}$. Assuming the period of the PN sequence is large, $\frac{1}{N} \ll 1$, the second term of Eq. (A.8) can be neglected so that Eq. (A.7) reduces to

$$e_\epsilon = P\left[\frac{2\epsilon}{T_c}\right] \quad (A.9)$$

Appendix B

Appendix B.1

The following three properties will be illustrated below:

- I. A maximal sequence has one more 1 than 0.
- II. The sum (modulo-2) of two phase-shifted versions of an m -sequence yields the same sequence but shifted.
- III. The discrete autocorrelation of an m -sequence is two-valued.

The seven bit binary number

0011101

has four ones and three zeros and is therefore consistent with the first mentioned property. The second property is exemplified by shifting the sequence two bits and adding (modulo-2)

• 0011101

1110100

1101001

It is noticed that the sum is shifted left from the original sequence by three bits but remains unaltered. The third stated property can be illustrated by recalling that the ones and zeros are represented by ± 1 so that

original sequence c_k : 0011101 \rightarrow -1 -1 1 1 1 -1 1

sequence shifted by k : 0011101 \rightarrow -1 -1 1 1 1 -1 1

product of these sequences: 1 -1 1 1 -1 -1 -1

$$R(kT_d) = E[c(t)c(t - kT_d)] = -\frac{1}{7}$$

where $k = \pm 1, \pm 2, \pm 3, \dots$

$$R(0) = E[c(t)c(t)] = E[c^2(t)] = \frac{7(1)}{7}$$

These two equations can be written succinctly (since they cover different regions) as

$$R_c(nT_d) = \begin{cases} 1 & n = 0, 7, 14, \dots \\ -1/7 & n = 0, 7, 14, \dots \end{cases} \quad (B.1)$$

This can be written in a more general form using the following definition for the discrete autocorrelation function:

$$r_c(t) = \frac{1}{N} \sum_{i=1}^N c_i c_{i+k} \quad (B.2)$$

where N is the period of the sequence. In the example, the amplitude of unity is used and $N = 7$ therefore Eq. (B.2) reduces to

$$r_c(t) = \begin{cases} 1 & k = 0, N, 2N, \dots \\ -1/N & \text{otherwise} \end{cases} \quad (B.3)$$

Appendix B.2

The PSD of one period of the autocorrelation function of a maximal-length sequence can be simplified as follows: Recall Eq. (2.30),

$$\begin{aligned}
S_{c_1}(f) &= \int_{-T_0/2}^{-T_c} -\frac{1}{N} \exp(-j2\pi f\tau) d\tau + \int_{T_c}^{T_0/2} \frac{-1}{N} \exp(-j2\pi f\tau) d\tau \\
&\quad + \int_{-T_c}^0 \left(1 + \frac{N+1}{T_0} \tau\right) \exp(-j2\pi f\tau) d\tau \\
&\quad + \int_0^{T_c} \left(1 - \frac{(N+1)}{T_0} \tau\right) \exp(-j2\pi f\tau) d\tau \\
&= \frac{-1}{N} \left[\int_{-T_0/2}^{-T_c} \exp(-j2\pi f\tau) d\tau + \int_{T_c}^{T_0/2} \exp(-j2\pi f\tau) d\tau \right] \\
&\quad + \int_{-T_c}^0 \left(1 + \frac{N+1}{T_0} \tau\right) \exp(-j2\pi f\tau) d\tau + \int_0^{T_c} \left(1 - \frac{(N+1)}{T_0} \tau\right) \exp(-j2\pi f\tau) d\tau \\
&= \frac{1}{Nj2\pi f} [e^{j2\pi fT_c} - e^{j2\pi fT_0/2} + e^{-j2\pi fT_0/2} - e^{-j2\pi fT_c}] \\
&\quad - \frac{1}{j2\pi f} [-e^{j2\pi fT_c} + e^{-j2\pi fT_c}] \\
&\quad + \frac{(N+1)}{T_0} \left[\int_{-T_c}^0 \tau e^{-j2\pi f\tau} d\tau - \int_0^{T_c} \tau e^{-j2\pi f\tau} d\tau \right] \\
&= \frac{1}{N\pi f} [\sin 2\pi fT_0/2] + \frac{1}{\pi f} \sin 2\pi fT_c \\
&\quad + \frac{(N+1)}{T_0} \left[\left. \frac{\tau e^{-j2\pi f\tau}}{-j2\pi f} \right|_{-T_c}^0 - \int_{-T_c}^0 \frac{e^{-j2\pi f\tau}}{-j2\pi f} d\tau \right. \\
&\quad \left. - \left. \frac{\tau e^{-j2\pi f\tau}}{-j2\pi f} \right|_0^{T_c} + \int_0^{T_c} \frac{e^{-j2\pi f\tau}}{-j2\pi f} d\tau \right] \\
&= \frac{1}{N\pi f} [\sin 2\pi fT_c - \sin \pi fT_0] + \frac{1}{\pi f} \sin 2\pi fT_c \\
&\quad + \frac{(N+1)}{-j2\pi fT_0} \left[T_c e^{j2\pi fT_c} + \frac{1 - e^{j2\pi fT_c}}{j2\pi f} - T_c e^{-j2\pi fT_c} - \frac{e^{-j2\pi fT_c} - 1}{j2\pi f} \right]
\end{aligned} \tag{B.4}$$

Substituting $T_0 = NT_c$ and simplifying yields

$$\begin{aligned}
S_{c_1}(f) &= \frac{-1}{N\pi f} \sin \pi fT_0 + \frac{(N+1)}{(\pi f)^2 T_0} \sin^2 \pi fT_c \\
&= -T_c \text{sinc} fT_0 + \frac{(N+1)}{N} T_c \text{sinc}^2 fT_c
\end{aligned} \tag{B.5}$$

Appendix B.3

In order to write the spectral density for the maximal-length sequence in a simplified form, Eq. (2.31),

$$S_{c_1}(f) = -T_c \text{sinc}(fNT_c) + \frac{(N+1)T_c}{N} \text{sinc}^2(fT_c) \quad (B.6)$$

must be substituted into Eq. (2.32) yielding,

$$S_c(f) = \frac{1}{N} \text{sinc}(fNT_c) \sum_{n=-\infty}^{\infty} \delta(f - \frac{n}{NT_c}) + \frac{N+1}{N^2} \text{sinc}^2(fT_c) \sum_{n=-\infty}^{\infty} \delta(f - \frac{n}{NT_c}) \quad (B.7)$$

Notice that the first term on the right-hand side can be reduced since it is only nonzero at $f = 0$ and the second term is kept in the same form so that the envelope of the discrete spectra can easily be seen. Eq. (B.7) can be simplified to

$$S_c(f) = -\frac{1}{N} \delta(f) + \frac{(N+1)}{N^2} \sum_{n=-\infty}^{\infty} \text{sinc}^2(fT_c) \delta(f - \frac{n}{NT_c}) \quad (B.8)$$

Bibliography

- [1] D.M. DiCarlo and C.L. Weber, Statistical Performance of Single Dwell Serial Synchronization Systems, IEEE Trans. Comm., COM-28, No. 8, pp. 1382-1388, August 1980
- [2] L.E. Franks, Carrier and Bit Synchronization in Data Communications - A Tutorial Review, IEEE Trans. Comm., COM-28, No. 8, pp. 1107-1121, August 1980
- [3] W.J. Gill and J.J. Spilker, An Interesting Decomposition Property for Self Products of Random or Pseudorandom Binary Sequences, IEEE Trans. Comm., pp.1246-1247, June 1963
- [4] S.J. Mason, Feedback Theory - Some properties of Signal Flow Graphs, Proc. IRE, vol. 41, pp.1144-1156, September 1953
- [5] S.J. Mason, Feedback Theory - Further properties of Signal Flow Graphs, Proc. IRE, vol. 44, pp. 920-926, July 1956
- [6] J.K. Holmes, Coherent Spread Spectrum Systems, New York: John Wiley and Sons, 1982
- [7] J.K. Holmes and C.C. Chen, Acquisition Time Performance of PN Spread Spectrum Systems, IEEE Trans. Comm., COM-25, pp. 778-783, August 1977
- [8] W.J. Gill, Effect of Synchronization Error in Pseudorandom Carrier Communications, Conference Record, 1st Annual IEEE Comm. Conf., June 1965
- [9] J. Kemeny and J. Snell, Finite Markov Chains, New York: Van Nostrand, 1960
- [10] D.M. DiCarlo and C.L. Weber, Multiple Dwell Serial Search: Performance and Application to Direct Sequence Code Acquisition, IEEE Trans. Comm., COM-31, No.5, pp.650-659, May 1983
- [11] H. Meyr and G. Polzer, Performance Analysis for General PN Spread Spectrum Acquisition Techniques, IEEE Trans Comm., COM-31, No.12, pp.1317-1319, December 1983
- [12] A. Polydoros and C. Weber, A Unified Approach to Serial Search Spread Spectrum Code Acquisition - Part I, II, IEEE Trans. Comm., COM-32, No.5, pp.642-660, May 1984
- [13] A. Papoulis, Probability, Random Variables and Stochastic Processes, New York: McGraw-Hill, 1984
- [14] M.K. Simon et al., Spread Spectrum Communications, Volume I, II, III, Maryland:Computer Science Press, 1985